DOT/FAA/AR-11/11

Federal Aviation Administration
William J. Hughes Technical Center
Aviation Research Division
Atlantic City International Airport
New Jersey 08405

Failure of Notched Laminates Under Out-of-Plane Bending

April 2017

Final Report

U.S. Department of Transportation
Federal Aviation Administration

NOTICE

Technical Report Documentation Page

1. Report No.	2. Government Accession No.	3. Recipient's Catalog No.
DOT/FAA/AR-11/11		

4. Title and Subtitle	5. Report Date
FAILURE OF NOTCHED LAMINATES UNDER OUT-OF-PLANE BENDING	April 2017
	6. Performing Organization Code

7. Author(s)	8. Performing Organization Report No.
T.C. Kennedy, J. Parmigiani, S.A. Gonzalez, and T.J. Luedeman	

9. Performing Organization Name and Address	10. Work Unit No. (TRAIS)
School of MIME Oregon State University Corvallis, OR 97331	11. Contract or Grant No.

12. Sponsoring Agency Name and Address	13. Type of Report and Period Covered
U.S. Department of Transportation Federal Aviation Administration Air Traffic Organization NextGen & Operations Planning Office of Research and Technology Development Washington, DC 20591	Final Report
	14. Sponsoring Agency Code AIR-100

15. Supplementary Notes

The Federal Aviation Administration William J. Hughes Aviation Research Division Technical Monitor was Lynn Pham.

16. Abstract

The design of aircraft structures made of composite materials is heavily influenced by damage tolerance requirements. The primary goal of this research was to develop analysis techniques that are useful for the design of composite aircraft structure subjected to general out-of-plane loading. This project was limited to the out-of-plane bending case and focused on some very basic experiments and modeling efforts involving simple structures (center-notched, unstiffened laminates) under pure bending. Failure modes of the laminates were investigated, and the capability of a currently existing analysis technique for predicting failures was evaluated. The experimental work involved testing notched laminates under four-point bending. Two notch lengths, two laminate thicknesses, and three-ply lay-ups were studied. Failure progression in thin laminates appeared to be different from thick laminates. Thin laminates exhibited negligible visible damage before failure, which was generally sudden and resulted in the laminate breaking into two pieces. Thick laminates exhibited a gradual progression of damage, which is usually confined to the compression side of the laminate. Also, delamination, followed by buckling of the plies between the delamination site and the surface on the compression side of the laminate, was an important failure mechanism for thick laminates. The primary effort was to model progressive damage in notched laminates under bending. The progressive damage model for composites in ABAQUS® was used to simulate the growth of the notch up to ultimate failure for each laminate tested. Two types of finite element models were constructed—one that allowed delamination between plies and another that did not. The one that did not allow delamination was reasonably accurate in predicting the failure load for the thin laminates but generally overestimated the failure load for the thick laminates. The model that allowed delamination was generally in better agreement with the test results for the thick laminates. The sensitivity of the laminate failure load to the parameters that go into the progressive damage model was also studied. It was found that the final failure load for notched laminates under bending is predominantly controlled by the ply properties in the fiber direction but is not sensitive to changes in these properties in that large changes in these properties tend to produce small changes in failure load. Initial failure is sensitive to these properties.

17. Key Words	18. Distribution Statement
Composites, Damage tolerance, Notched laminates, Out-of-plane bending, Analysis	This document is available to the U.S. public through the National Technical Information Service (NTIS), Springfield, Virginia 22161. This document is also available from the Federal Aviation Administration William J. Hughes Technical Center at actlibrary.tc.faa.gov.

19. Security Classif. (of this report)	20. Security Classif. (of this page)	21. No. of Pages	22. Price
Unclassified	Unclassified	60	

ACKNOWLEDGEMENTS

This work was funded through the FAA Joint Advanced Materials and Structures Center of Excellence, with Curtis Davies and Lynn Pham as project monitors, and by The Boeing Company. The authors would like to express their appreciation for technical guidance provided by Gerald Mabson of Boeing, Thomas Walker of NSE composites, and Larry Ilcewicz of the FAA.

TABLE OF CONTENTS

LIST OF FIGURES

LIST OF TABLES

LIST OF ACRONYMS

FEA	Finite element analysis
KPT	Kirchhoff Plate Theory
RPT	Reissner Plate Theory
VCCT	Virtual Crack Closure Technique

EXECUTIVE SUMMARY

Damage tolerance requirements have a major influence on the design of aircraft structures made of composite materials. Numerous studies have been devoted to the problem of predicting failure in notched laminates. These investigations have generally focused on the response of laminates to in-plane tension, compression, or shear. However, out-of-plane bending, twisting, or shear is a reasonably common load situation in aircraft structures. For example, in an aircraft fuselage, the skin experiences this type of load in the vicinity of stiffening members, such as frames and stringers. Very little research has been devoted to this topic. The primary goal of this research was to develop analysis techniques that are useful for the design of composite aircraft structure subjected to general out-of-plane loading. This project was limited to the out-of-plane bending case and focused on some very basic experiments and modeling efforts involving simple structures (center-notched, unstiffened laminates) under pure bending. In partnership with The Boeing Company, Oregon State University investigated the failure modes of the laminates and evaluated the capability of some currently existing analysis techniques for predicting failures. The project was divided into five main tasks.

Task 1 involved testing notched laminates under four-point bending. Two notch lengths were considered: a 1-inch-long ovaloid hole with a 0.125-inch end radius and a 4-inch-long ovaloid hole with a 0.125-inch end radius. Two laminate thicknesses were studied: 20 and 40 plies. For each thickness, three laminate types were studied: one with 10% 0° plies, one with 30% 0° plies, and one with 50% 0° plies. The moment required for failure was measured for each specimen. During the tests, the 20-ply laminates exhibited negligible visible damage before failure, which was sudden and usually resulted in the laminate breaking into two pieces. The 40-ply laminates exhibited a gradual progression of damage that usually began with wrinkling of the outer ply on the compression side. This was followed by delamination at the outermost 0° ply and fracture of the plies between the outermost 0° ply and the surface. There was also some delamination between the second outermost 0° ply and the surface. The tension side of the laminate generally exhibited considerably less visible damage. In some cases, it was observed that the plies between the outermost 0° ply and the surface buckled before fracturing.

Task 2 involved modeling stress concentrations in notched laminates under bending. The general purpose finite element analysis program ABAQUS® was used to construct models of each laminate tested under four-point bending. Individual plies were modeled using two 3-D solid elements through the thickness of each ply. Less detailed models were also constructed using conventional shell elements to determine the level needed for acceptable accuracy. The elastic strain concentration factor near the notch was influenced by transverse shear effects, and these should be included in finite element models. Three-dimensional, free-edge effects were also evident, but these effects dissipated rapidly with distance from the edge.

Task 3 involved evaluating several semi-empirical failure models to be used for the preliminary design of the out-of-plane bending case. These models have been shown to be useful in estimating failure loads for notched laminates for the in-plane tension case. The point stress, point strain, and modified singularity criteria were examined. The point stress criterion predicted failure to occur when the stress at some critical distance (d) ahead of the notch tip reaches the unnotched strength of the laminate. The point strain criterion was similar but used strain values rather than stress. The modified singularity method used classical fracture mechanics but with a

material-dependent singularity value rather than the traditional square root. After modifying these theories to account for bending and applying the test results, they did not appear to be effective tools for using small notch data to predict failure for laminates with larger notches under bending.

Task 4 involved modeling progressive damage in notched laminates under bending. The progressive damage model for composites in ABAQUS was used to simulate the growth of the notch up to ultimate failure for each laminate tested in four-point bending. This provided a test of the validity of this model for a loading condition that was not considered previously. Two types of finite element models were constructed—one that allowed delamination between plies and another that did not. The one that did not allow delamination was reasonably accurate in predicting the failure load for the 20-ply laminates but generally overestimated the failure load for the 40-ply laminates. This was expected because only the 40-ply laminates exhibited delamination as an important failure mechanism in the tests. The model that allowed delamination was generally in better agreement with the test results for the 40-ply laminates. These models also showed good agreement with the test results for the 20-ply laminates. The overall conclusion was that the progressive damage model appears to be a useful tool in predicting failure in notched laminates under bending and is capable of replicating a complex delamination response.

Task 5 involved a study of the sensitivity of the laminate failure load to the parameters that go into the progressive damage model. This was accomplished by performing a systematic series of numerical experiments using design-of-experiments methodology. The overall conclusion from these results is that the final failure of notched laminates under bending is dominated by the ply properties in the fiber direction. Also, large changes in these properties (±20%) tend to produce small changes in failure load (<±7%). The relatively low sensitivity of failure load to these properties is a desirable outcome because it indicates a progressive damage analysis will not require that highly accurate values of these properties be determined experimentally. Initial failure is sensitive to these properties.

1. INTRODUCTION

The design of aircraft structures made of composite materials is heavily influenced by damage tolerance requirements. The problem of predicting failure in notched laminates has been the subject of numerous studies. In general, these investigations focused on the response of laminates to in-plane tension, compression, or shear. However, out-of-plane bending, twisting, or shear can be present. For example, in an aircraft fuselage, the skin will experience this type of load in the vicinity of stiffening members, such as frames and stringers. Very little research has been devoted to this topic [1–4]. As a result, the response of notched laminates subjected to out-of-plane loads is not well understood. This uncertainty could lead to unnecessarily conservative design.

Analysis techniques are needed that are useful for the design of composite aircraft structures under out-of-plane loading. The development of these techniques is complicated by several factors. First, for out-of-plane loading, the laminate does not experience a uniform strain through its thickness as in the in-plane loading case. This likely results in progressive damage development up to final failure that is quite different from the in-plane loading case. In homogeneous metal structures, all failure modes (I, II, and III) can occur simultaneously at the notch tip during combined bending and shear or twist. The composite laminate case would be expected to be even more complex. Models capable of simulating this behavior will likely require an unusual degree of sophistication. Also, the development of analysis techniques requires significant experimental support to guide the development of the theoretical models. Unfortunately, there is very little test data currently available for the out-of-plane loading case.

The primary goal of this research was to develop analysis techniques that are useful for the design of composite aircraft structure subjected to general out-of-plane loading. These techniques should be accurate, efficient, and suitable for implementation into existing design methodology. The various analytical models that are developed must have the appropriate level of sophistication to meet the designer's needs from simple hand calculations to computer simulation of complex, ply-level response exhibiting multiple failure modes. The models also need to be thoroughly validated through tests from small coupons to large configured structure. The realization of this goal is beyond the scope of a single project. The focus in this study was on some very basic experiments and modeling efforts involving simple structures (center-notched, unstiffened laminates) under pure bending. For a limited number of tests, the modes of failure of the laminates were determined and the capability of a currently existing analysis technique for predicting these failures was evaluated.

Accomplishing the objective required both experimental and computational efforts. The project was divided into five main tasks.

1. Task 1 involved testing notched laminates under four-point bending. Two notch lengths were considered: a 1-inch-long ovaloid hole with a 0.125-inch end radius and a 4-inch-long ovaloid hole with a 0.125-inch end radius. Two laminate thicknesses were studied: 20 and 40 plies. For each thickness, three laminate types were studied: one with 10% 0° plies, one with 30% 0° plies, and one with 50% 0° plies. The failure moment was measured for each specimen. The material used to fabricate the test specimens was provided by the Boeing Corporation. It was a direct representation of the materials and

lay-ups used in their products and therefore considered company proprietary. Though this precludes the release of the raw test data from this task, it did ensure that data, and the limits of validity of the models created from the data, covered the space of interest.

2. Task 2 involved modeling stress concentrations in notched laminates under bending. The general purpose finite element analysis (FEA) program ABAQUS® was used to construct models of each of the laminates tested under four-point bending. Individual plies were modeled using two 3-D solid elements through the thickness of each ply. Less detailed models were also constructed using conventional shell elements to determine the level needed for acceptable accuracy.
3. Task 3 involved evaluating several semi-empirical failure models to be used for preliminary design for the out-of-plane bending case. These types of models have been shown to be useful in estimating failure loads for notched laminates for the in-plane tension case.
4. Task 4 involved modeling progressive damage in notched laminates under bending. The progressive damage model for composites in ABAQUS was used to simulate the growth of the notch up to ultimate failure for each laminate tested in four-point bending. This has provided a validity test of this model for a loading condition that was not considered previously.
5. Task 5 involved a study of the sensitivity of the laminate failure load to the parameters that go into the progressive damage model. This was accomplished by performing a systematic series of numerical experiments using a design of experiments methodology.

The results for Task 2 through Task 5 are described in the following sections. The results for Task 1 are not separately presented but are discussed in the context of the other tasks. This is because of the proprietary nature of most of that data as described above.

2. TASK 2: MODELING STRESS CONCENTRATIONS IN NOTCHED LAMINATES UNDER BENDING

For design to ultimate load, stress concentration factors are needed for notches around configured structure. The analysis of stresses around notches in plates subjected to out-of-plane bending has been the subject of a number of investigations. Typically, this analysis consists of a plate (usually of infinite extent) with thickness (h) containing a notch. The typical loading situation consists of a uniform bending moment (M_o) in one direction. Analyses have been carried out using two plate theories: Kirchhoff Plate Theory (KPT), which ignores the effect of transverse shear deformation (this is also referred to as classical theory), and Reissner Plate Theory (RPT), which accounts for the effect of transverse shear deformation. For uniform bending of a homogeneous, isotropic plate, the far-field normal stress is linear through the thickness with a maximum value at the plate surface of

$$\sigma_b = \frac{6M_o}{h^2} \tag{1}$$

At the notch, a stress concentration is normally expressed as $\sigma_{max} = k_b\sigma_b$. Using KPT, Goodier [5] studied stresses around a circular hole with radius (a) in an isotropic plate and found the stress concentration factor as

$$k_b = \frac{5+3\nu}{3+\nu} \tag{2}$$

where ν is Poisson's ratio. Reissner [6] developed his theory taking transverse shear deformation effects into account and found

$$k_b = \frac{3}{2} + \frac{1}{2}\frac{3(1+\nu)K_2(\mu)/2 - K_0(\mu)}{(1+\nu)K_2(\mu)/2 + K_0(\mu)} \tag{3}$$

where $\mu = (10)^{1/2}a/h$ and K_0 and K_2 are modified Bessel functions. Here, the stress concentration factor depends on a/h, as shown in figure 1, where k_b varies between 3 for a very thick plate (a/h small) to Goodier's KPT result for a very thin plate for ν = 1/4. A 3-D elasticity solution developed by Alblas [7] is also shown in figure 1. Improvements to the theory were later presented by Lee [8] and Reissner [9]. Goodier [5] also studied stresses around an elliptical hole (with major axis a and minor axis b) in an isotropic plate using KPT and found the stress concentration factor as

$$k_b = 1 + \frac{2(1+\nu)a/b}{3+\nu} \tag{4}$$

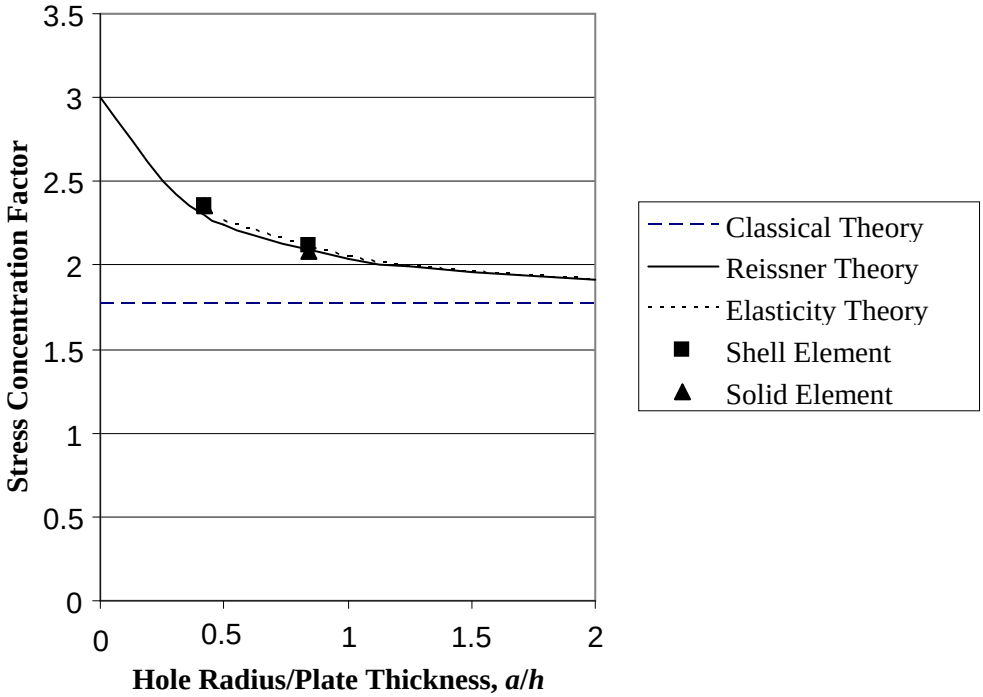

Figure 1. Stress concentration factor for a homogeneous, isotropic plate under bending

Naghdi [10] studied the same case using RPT and was able to determine an approximate value for k_b in terms of Mathieu functions for the case when the elliptical hole is not too slender.

The results described above are not directly applicable to notched laminates because of the anisotropic nature of these materials. The extension of KPT to orthotropic materials is reasonably straightforward. The case of a circular hole in an orthotropic plate under bending was studied by Leknitskii [11] where k_b is given as

$$k_b = 1 + \frac{kn}{k + 4g} \tag{5}$$

where k, n, and g are functions of the flexural moduli D_{11}, D_{22}, D_{12}, and D_{66}. Prasad and Shuart [12] extended Leknitskii's [11] results to the case of an elliptical hole in an orthotropic plate. Here, the solution is sufficiently complex that it is not possible to develop an explicit expression for k_b. Material anisotropy was found to have a significant effect on the stress concentration factor. The extension of RPT to orthotropic materials usually does not allow for analytical solution and requires an FEA. Paul and Rao [13 and 14] performed such analyses for a finite, simply supported plate under a uniform pressure containing either a circular or elliptical hole.

For the case when the notch is a sharp crack, Zendher and Viz [15] give a summary of results using KPT for isotropic materials. Here, the stress intensity factor is

$$k_1 = \frac{6M_o}{h^2}\sqrt{a} = \sigma_b\sqrt{a} \tag{6}$$

Results for RPT are given in Wu and Erdogan [16] for ν = 0.3. They found that k_1 depends on a/h, with $k_1 = \sigma_b a^{1/2}$ for $a/h \to 0$ and $k_1 = 0.63\ \sigma_b a^{1/2}$ for $a/h \to \infty$. Simmonds and Duva [17] concluded that the strain energy release rates calculated from KPT and RPT should be the same as $a/h \to \infty$. This led to the conclusion that the k_1's for the two theories should differ by a factor of $[(1 + \nu)/(3 + \nu)]^{1/2}$, which is equal to 0.63 for ν = 0.3. Wu and Erdogan [16] also considered the orthotropic material case and found that orthotropy can have a significant influence on the stress-intensity factor.

For aircraft structures made of composite materials, designers have traditionally relied on Leknitskii's [11] work (which is based on KPT), because of the availability of analytical solutions. The objective of the current study is to investigate the validity of this approach by comparing the results from KPT to those from the more accurate solutions provided by RPT and 3-D elasticity theory. This was accomplished by performing finite element analyses using the commercial program ABAQUS on laminates with several different types of notches as described in the following sections.

2.1 FINITE ELEMENT MODELS

A variety of notch sizes ranging from small fastener holes to larger-scale penetration damage were modeled. Three different notch types were analyzed: a 0.25-inch-diameter hole, a 1-inch-long ovaloid, and a 4-inch-long ovaloid in laminates under pure bending. The ovaloids were slits with rounded tips (0.125-inch radius) and represent blunt, crack-type notches (see figure 2). This provided a 0.25-inch gap between the surfaces of the slit, which prevented the surfaces from coming into contact on the compression side of the laminate during bending. Six different laminates were investigated, including two laminate thicknesses: 20 and 40 plies. For each thickness, three laminate types were studied: one with 10% 0° plies, one with 30% 0° plies, and one with 50% 0° plies.

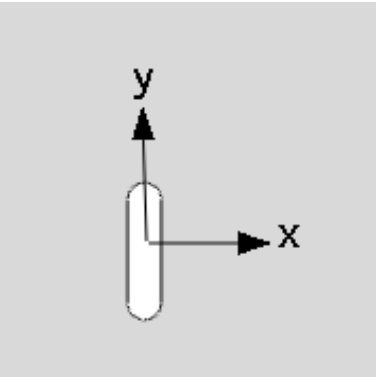

Figure 2. Ovaloid notch in a plate

Three types of finite element models were constructed: (1) shell elements without transverse shear effects, (2) shell elements with transverse shear effects, and (3) quadratic 3-D continuum

solid elements with two elements through the thickness of each ply (using more than two elements through the thickness of each ply was found to have negligible effect of the solution). The mesh for the 20-ply laminate with a 0.25-inch-diameter hole modeled with 3-D solid elements is shown in figure 3, where one-half of the plate is modeled. Although this symmetry assumption is not strictly valid because of weak coupling between bending and twisting, it has a negligible effect on the strain concentration. The plate width-to-hole diameter ratio is 10. To save computing time, the region on the plate away from the hole was modeled with shell elements with appropriate coupling constraints across the solid-shell interface (modeling the entire laminate with solid elements gave results that were within 1 percent of those of the current model). The meshes for laminates with a 1-inch-long notch and a 4-inch-long notch are shown in figures 4 and 5, respectively. The mesh for the laminates modeled completely with shell elements had the same planar density as the solid element meshes. To verify the models, a calculation was performed on a homogeneous, isotropic material with a circular hole (the values obtained using the shell element model with transverse shear effects and the 3-D solid element model for the two thicknesses considered are compared with the analytical solutions in figure 1). The slight difference between the FEA results and the analytical solutions is likely due to finite width effects.

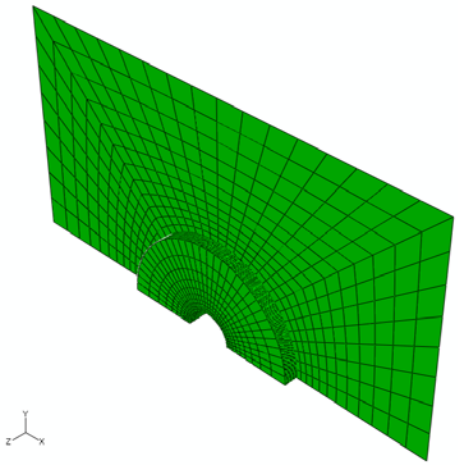

Figure 3. Finite element mesh for the 20-ply laminate

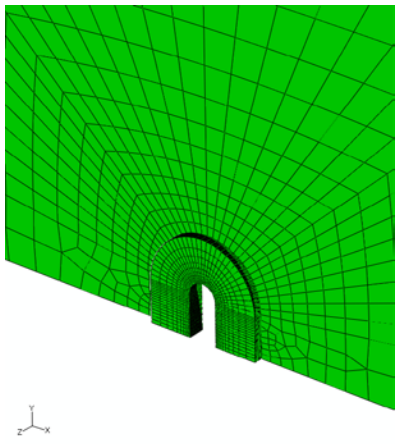

Figure 4. Finite element mesh for a 1-inch-long notch

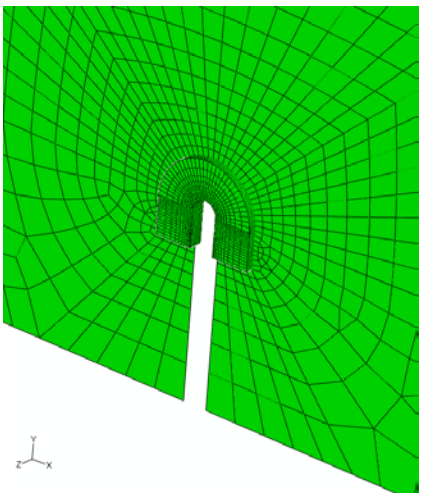

Figure 5. Finite element mesh for a 4-inch-long notch

2.2 RESULTS

Because of the discontinuous nature of the stress distribution through the thickness of the laminate, it is probably more useful to consider strain concentration factors rather than stress concentration factors. In composite aircraft design, the strain in the outermost 0° ply is frequently used as a design limiter. Therefore, the focus was on the strain in this ply. The strain distributions through the thickness of the 20-ply laminate with 10% 0° plies at the edge of the 0.25-inch-diameter hole from both the 3-D solid model and the two shell models are shown in figure 6. As expected, the strains from the shell models are linear through the thickness. The strain from the 3-D solid model is nearly linear, except for two pronounced bulges in the location of the 0° plies. The strain distribution predicted by the 3-D solid model appears to be a free-edge effect (where singularities in stress are known to exist at ply interfaces). This becomes apparent when observing the strain distribution through the thickness predicted by the three models at a point 0.025-inch away from the edge of the hole. This is shown in figure 7. Here, the three strain distributions are in relatively good agreement. This same conclusion can be reached by examining the results for the 40-ply laminate. The discrepancy in results predicted by the 3-D solid model and the shell models is quite likely caused by a free-edge effect. It is known that singularities in transverse shear and normal stresses exist at ply interfaces on a free edge. These large stresses would render invalid the usual assumptions of plate theory. Several other laminated plate theory assumptions that involve neglecting gradients in the twisting moment may also be violated. Therefore, it is not surprising that the results would differ.

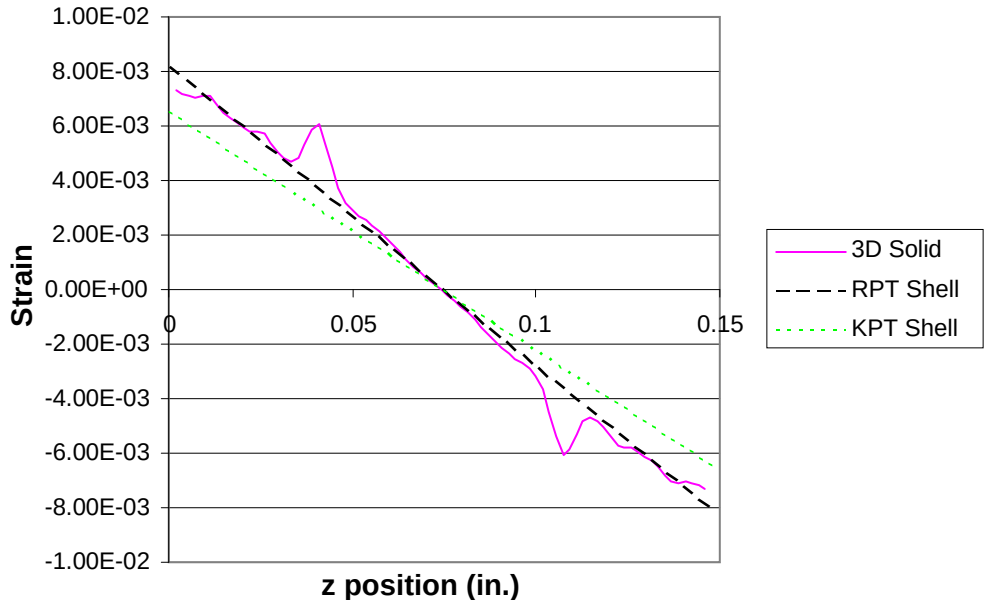

Figure 6. Strain distributions through the thickness at the edge of a 0.25-inch-diameter hole in a 20-ply laminate with 10% 0° plies

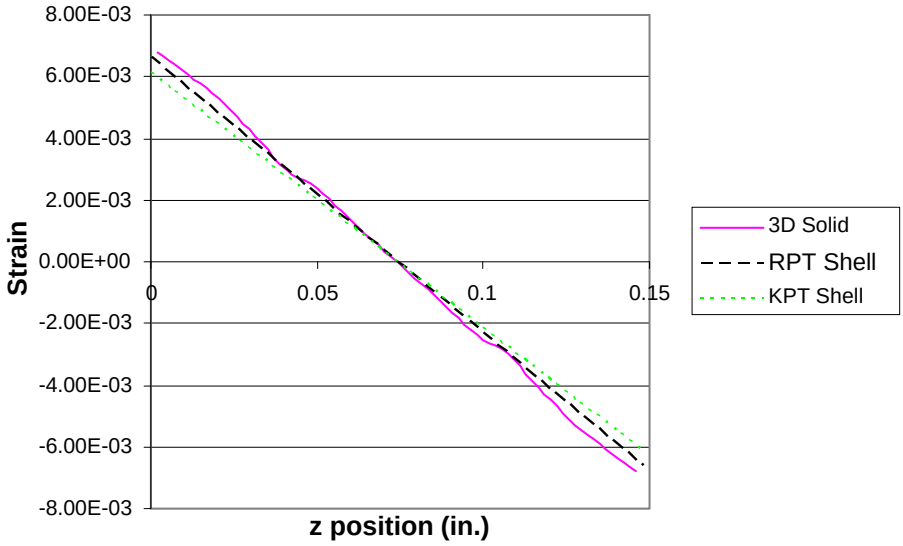

Figure 7. Strain distributions through the thickness at a point 0.025 inch away from the edge of a 0.25-inch-diameter hole in a 20-ply laminate with 10% 0° plies

A strain concentration factor was calculated based on the maximum strain the in outermost 0° ply for each laminate and notch size using the three types of models. These results are shown in figures 8–13. In each case, the 3-D solid model predicted a higher strain concentration factor than the two shell models. For the 0.25-inch-diameter hole, the strain concentration factor predicted by the shell model with transverse shear effects was, on average, 38% higher than what was predicted by the shell model without transverse shear effects. For the 1-inch-long notch, it was 31% higher. For the 4-inch-long notch, it was 23% higher. For the 0.25-inch-diameter hole, the strain concentration factor predicted by the 3-D solid model was, on average, 100% higher

than what was predicted by the shell model without transverse shear effects. For the 1-inch-long notch, it was 76% higher. For the 4-inch-long notch, it was 62% higher.

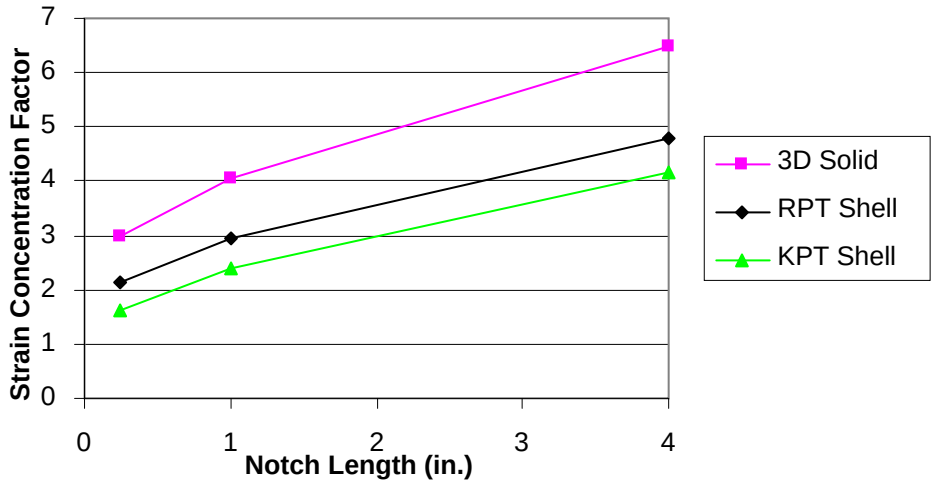

Figure 8. Strain concentration factor vs notch length for a 20-ply laminate with 10% 0° plies

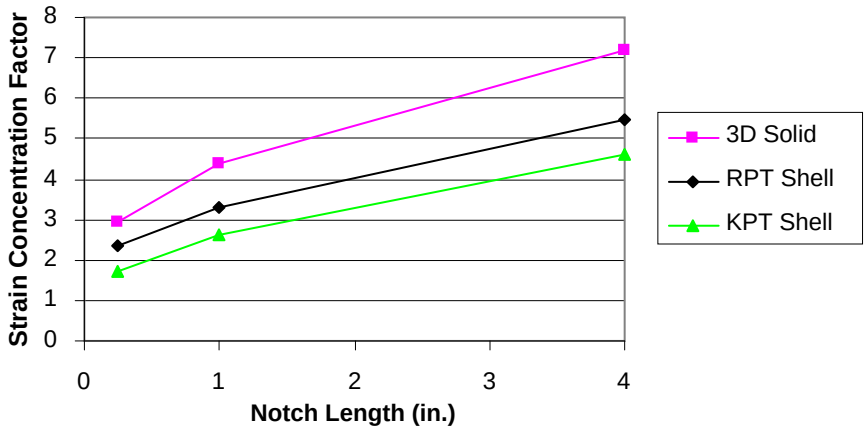

Figure 9. Strain concentration factor vs notch length for a 20-ply laminate with 30% 0° plies

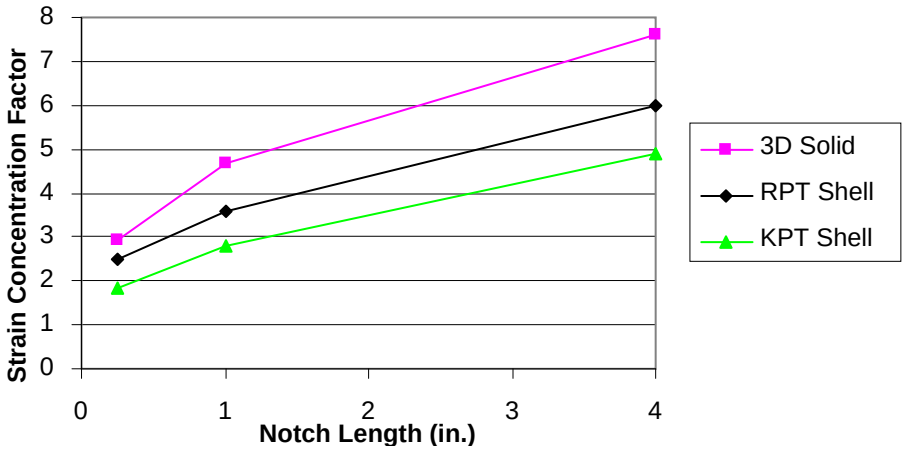

Figure 10. Strain concentration factor vs notch length for a 20-ply laminate with 50% 0° plies

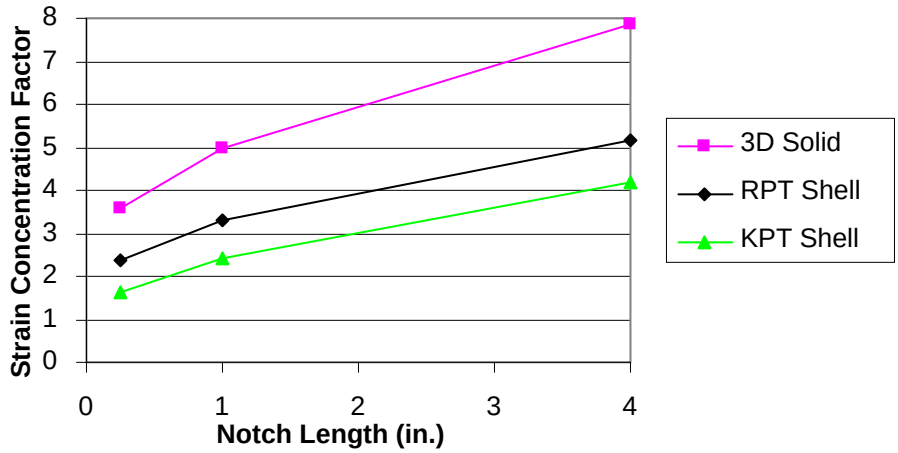

Figure 11. Strain concentration factor vs notch length for a 40-ply laminate with 10% 0° plies

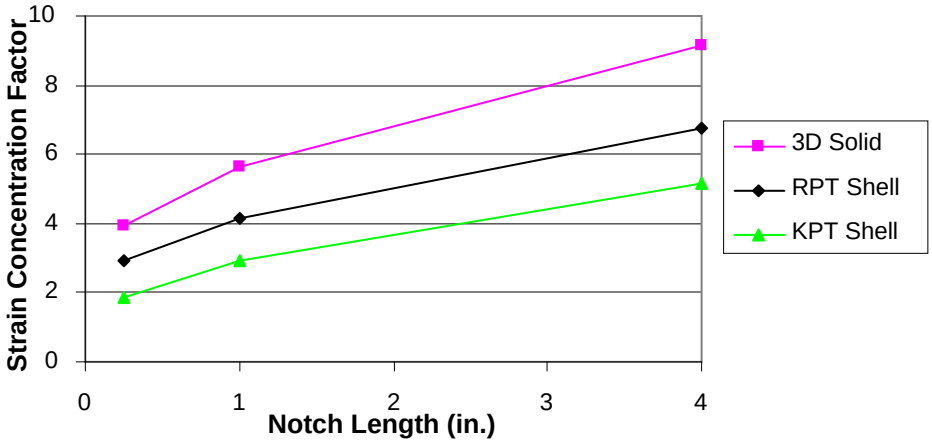

Figure 12. Strain concentration factor vs notch length for a 40-ply laminate with 30% 0° plies

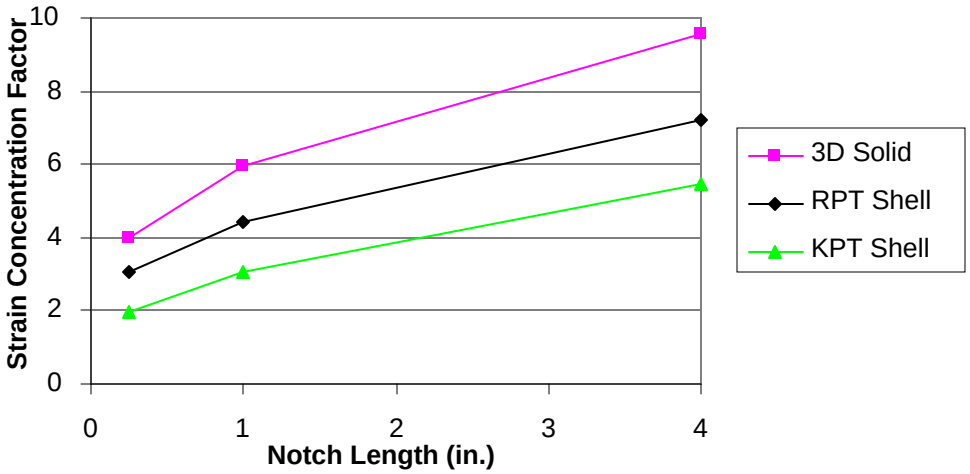

Figure 13. Strain concentration factor vs notch length for a 40-ply laminate with 50% 0° plies

3. TASK 3: EVALUATION OF SEMI-EMPIRICAL MODELS

3.1 THEORY

Several semi-empirical failure criteria have been shown to be useful in estimating failure loads for notched laminates for the in-plane tension case [18]. The most commonly used are the point stress, point strain, and modified singularity criteria. The point stress criterion, developed by Whitney and Nuismer [19 and 20], predicts failure to occur when the stress at some critical distance (d) ahead of the notch tip reaches the unnotched strength of the laminate. The point strain criterion, developed by Poe and Sova [21 and 22], is similar but uses strain values rather than stress. The modified singularity method developed by Mar and Lin [23 and 24] uses classical fracture mechanics but with a material-dependent singularity value rather than the traditional square root.

The usefulness of this type of model for preliminary design was reported [25] for the out-of-plane bending case. This requires formulas for the internal bending moments per unit length in the vicinity of a notch in an orthotropic plate under bending. The solution to this problem using classical plate theory was developed by Prasad and Shuart [12]. They considered the case of an elliptical hole in an infinite plate, as shown in figure 14. They used complex variable techniques to solve the plate equation

$$D_{11}\frac{\partial^4 w}{\partial x^4}+4D_{16}\frac{\partial^4 w}{\partial x^3\partial y}+2(D_{12}+2D_{66})\frac{\partial^4 w}{\partial x^2\partial y^2}+4D_{26}\frac{\partial^4 w}{\partial x\partial y^3}+D_{22}\frac{\partial^4 w}{\partial y^4}=0 \qquad (5)$$

where w is the transverse displacement and D_{11}, D_{12}, D_{22}, D_{16}, D_{26}, and D_{66} are the terms from the bending stiffness matrix that relates the internal bending moment per unit length matrix $\{M\}$ to the plate curvature matrix $\{\kappa\}$ through the equation

$$\{M\}=[D]\{\kappa\} \qquad (6)$$

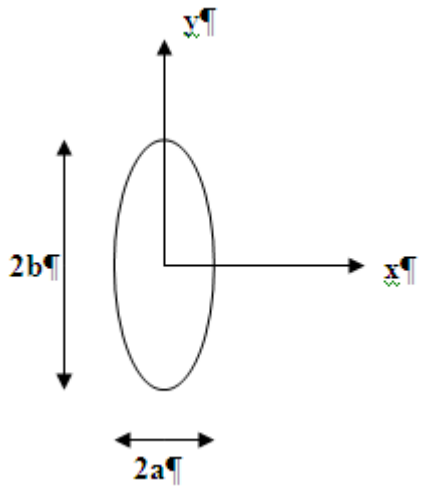

Figure 14. Elliptical hole in a plate under bending

The interest here is in the case where the far-field loading is such that $M_x = M_0$, $M_{xy} = 0$, and $M_y = 0$. For this case, the internal bending moments are

$$M_x = M_0\{1 - 2\,\mathrm{Re}[\,p_1\varphi(z_1) + q_1\psi(z_2)]\} \tag{7}$$

$$M_y = -2M_0\,\mathrm{Re}[\,p_2\varphi(z_1) + q_2\psi(z_2)] \tag{8}$$

where z_1 and z_2 are complex variables defined as

$$z_1 = x + s_1 y, z_2 = x + s_2 y \tag{9}$$

and s_1 and s_2 are roots of the characteristic equation

$$D_{22}s^4 + 4D_{26}s^3 + 2(D_{12} + 2D_{66})s^2 + 4D_{16}s + D_{11} = 0 \tag{10}$$

given as

$$s_1 = \alpha_1 + i\beta_1 \qquad s_2 = \alpha_2 + i\beta_2 \qquad s_3 = \overline{s}_1 \qquad s_4 = \overline{s}_2 \tag{11}$$

$\varphi(z_1)$ and $\psi(z_2)$ are complex functions defined as

$$\varphi(z_1) = \frac{N_1}{a + is_1 b}\left[1 - \frac{z_1}{[z_1^2 - (a^2 + s_1^2 b^2)]^{1/2}}\right] \tag{12}$$

$$\psi(z_2) = \frac{N_2}{a + is_2 b}\left[1 - \frac{z_2}{\left[z_2^2 - (a^2 + s_2^2 b^2)\right]^{1/2}}\right] \tag{13}$$

where

$$N_1 = \frac{s_1}{2(p_1 q_2 s_2 - p_2 q_1 s_1)}\left[\begin{array}{l}(A+iB)\left(p_2 q_1 - \dfrac{p_1 q_2 s_2}{s_1}\right)(a + is_1 b) + (A - iB)\left(\overline{p}_2 q_1 - \dfrac{\overline{p}_1 q_2 s_2}{\overline{s}_1}\right)(a + i\overline{s}_1 b) \\ +(C - iD)\left(q_1 \overline{q}_2 - \dfrac{q_2 \overline{q}_1 s_2}{\overline{s}_2}\right)(a + i\overline{s}_2 b)\end{array}\right] \tag{14}$$

$$N_2 = \frac{-s_2}{2(p_1 q_2 s_2 - p_2 q_1 s_1)}\left[\begin{array}{l}(A-iB)\left(p_1 \overline{p}_2 - \dfrac{p_2 \overline{p}_1 s_1}{\overline{s}_1}\right)(a + i\overline{s}_1 b) + (C + iD)\left(p_1 q_2 - \dfrac{p_2 q_1 s_1}{s_2}\right)(a + is_2 b) \\ +(C - iD)\left(p_1 \overline{q}_2 - \dfrac{p_2 \overline{q}_1 s_1}{\overline{s}_2}\right)(a + i\overline{s}_2 b)\end{array}\right] \tag{15}$$

$$p_1 = D_{11} + D_{12} s_1^2 + 2 s_1 D_{16} \tag{16}$$

$$p_2 = D_{12} + D_{22} s_1^2 + 2 s_1 D_{26} \tag{17}$$

$$p_3 = D_{16} + D_{26} s_1^2 + 2 s_1 D_{66} \tag{18}$$

$$p_4 = D_{11} / s_1 + 3 D_{16} + s_1 (D_{12} + 2 D_{66}) + D_{26} s_1^2 \tag{19}$$

$$q_1 = D_{11} + D_{12} s_2^2 + 2 s_2 D_{16} \tag{20}$$

$$q_2 = D_{12} + D_{22} s_2^2 + 2 s_2 D_{26} \tag{21}$$

$$q_3 = D_{16} + D_{26} s_2^2 + 2 s_2 D_{66} \tag{22}$$

$$q_4 = D_{11} / s_2 + 3 D_{16} + s_2 (D_{12} + 2 D_{66}) + D_{26} s_2^2 \tag{23}$$

and A, B, C, and D are solutions to the set of equations

$$-2\,\mathrm{Re}[\,p_1 (A + iB) + q_1 (C + iD)] = 1 \tag{24}$$

$$-2\,\mathrm{Re}[\,p_2 (A + iB) + q_2 (C + iD)] = 0 \tag{25}$$

$$-2\,\mathrm{Re}[\,p_3(A+iB)+q_3(C+iD)]=0 \tag{26}$$

$$-2\,\mathrm{Re}[\,p_4(A+iB)+q_4(C+iD)]=0 \tag{27}$$

A computer program was written to solve equations 24–27 and evaluate the internal bending moments per unit length in equations 7 and 8. Next, the concepts from references 19–24 were extended from the tension loading case to the out-of-plane bending case to compute the failure loads. The notch was assumed to be a crack (i.e., a = 0; this assumption is required to apply the point strain criterion and modified singularity criterion). A comparison of the results from tension and bending are given below.

- Point Stress Criterion (Whitney-Nuismer)

  Tension

$$\sigma_n=\sigma_u\sqrt{1-\frac{b^2}{(b+d)^2}} \tag{28}$$

  Bending

$$M_n=\frac{M_u}{\left[1-2c_1\left(1-\dfrac{b+d}{\sqrt{(b+d)^2-b^2}}\right)\right]} \tag{29}$$

$$c_1=\mathrm{Re}\left(\frac{p_1N_1}{is_1b}+\frac{q_1N_2}{is_2b}\right)$$

- Point Strain Criterion (Poe-Sova)

  Tension

$$\sigma_n=\frac{\sigma_u}{\sqrt{1+\dfrac{\xi^2b}{2d}}} \tag{30}$$

$$\xi=1-\nu_{xy}\sqrt{\frac{E_x}{E_y}}$$

Bending

$$M_n = \frac{M_u}{\sqrt{1+\frac{\xi^2 b}{2d}}}$$

$$\xi = 2\left(c_1 + c_2 \frac{d_{12}}{d_{11}} \right) \tag{31}$$

$$c_2 = \mathrm{Re}\left(\frac{p_2 N_1}{i s_1 b} + \frac{q_2 N_2}{i s_2 b} \right)$$

- Modified Singularity Criterion (Mar-Lin)

  Tension

$$\sigma_n = \frac{H}{b^n} \tag{32}$$

  Bending

$$M_n = \frac{H}{b^n} \tag{33}$$

where σ_n is the notched tensile strength, σ_u is the unnotched tensile strength, M_n is the notched bending strength, and M_u is the unnotched bending strength. The crack half-length is b, d is a characteristic length that is a material property, and d_{11} and d_{12} are terms from the inverse of matrix [D]. H is the laminate fracture toughness, and n is the order of the singularity at the crack tip. In each case, the notched bending strength has the same form as its tension counterpart.

3.2 COMPARISON OF THEORY AND TEST RESULTS

Each criterion contains empirical parameters that must be determined from test results. The point stress and point strain criteria require values for M_u and d; but the modified singularity criterion requires values for H and n. The results from tests on two types of laminates: one with 50% 0° plies and the other with 30% 0° plies were used. Both laminates were 20 plies thick. The notched bending strength M_n was determined from experiments on laminates with two notch lengths: 1 and 4 inches (the notches in the tests were ovaloids with 0.125-inch end radii rather than sharp cracks [see section 4.1]). From these results the empirical parameters were calculated[*]. Then, plots of notched bending strength M_n versus notch length $2b$ were generated for the two types of laminates, as shown in figures 15 and 16.

[*]This approach is backward compared to the traditional approach of determining M_u from a coupon test on an unnotched specimen, followed by determining d from a test on a specimen with a 0.25-inch-diameter hole. The traditional approach was not used because it would have required disclosure of confidential information from the Boeing database.

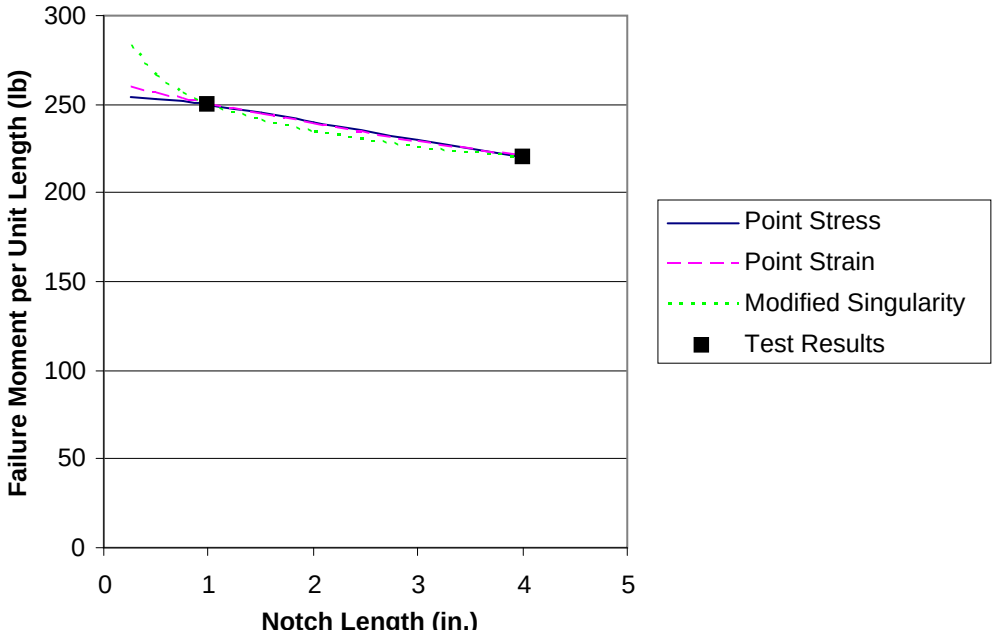

Figure 15. Failure moment vs notch length for a laminate with 50% 0° plies

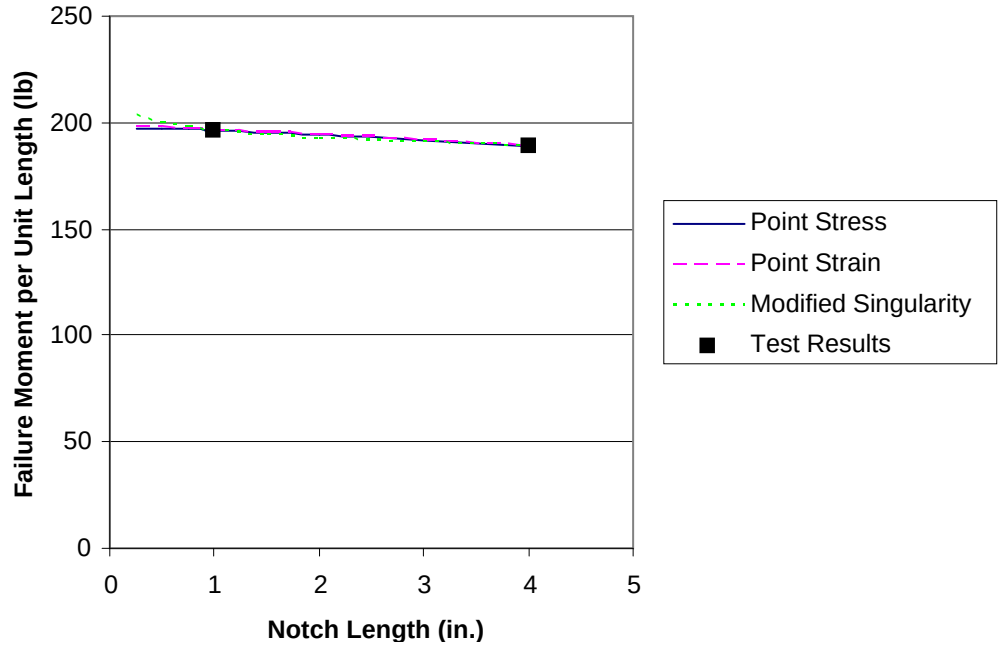

Figure 16. Failure moment vs notch length for a laminate with 30% 0° plies

Though the point strain and modified singularity criteria require the assumption of the notch being a sharp crack, the point stress criterion allows for the possibility of the notch being an ellipse. Although the notches in these tests were ovaloids rather than ellipses, it is common practice to calculate the stress concentration factor for an ovaloid using an equivalent ellipse that has the same length and same tip curvature as the ovaloid. Repeating the calculations for this case had negligible effect on the results.

4. TASK 4: MODELING PROGRESSIVE DAMAGE IN NOTCHED LAMINATES UNDER BENDING

4.1 TEST SETUP

Tests were performed on center-notched, unstiffened laminates consisting of three laminate types (10% 0°, 30% 0°, and 50% 0° plies), two laminate thicknesses (20 and 40 plies), and two notch lengths (1 and 4 inches). The notches were in the shape of ovaloid slits with an end radius of 0.125-inch Specimen geometry is shown in figure 17[1]. There were 12 different specimen types consisting of the laminate type, laminate thickness, and notch length. Three replicates of each specimen were fabricated with a specimen width-to-notch length ratio of five. The aspect ratio of the test area varied from 2 to 1/2. The laminates were subjected to four-point bending, as shown in figure 18. Several test fixtures were fabricated similar to the one shown in figure 18. The need for different fixtures was the result of several factors, including the need to accommodate very large displacements (>6 inches) for some laminates and large loads (>10,000 lb) for others. The fixtures were similar in that they applied load to the laminates through 1-inch-diameter aluminum bars.

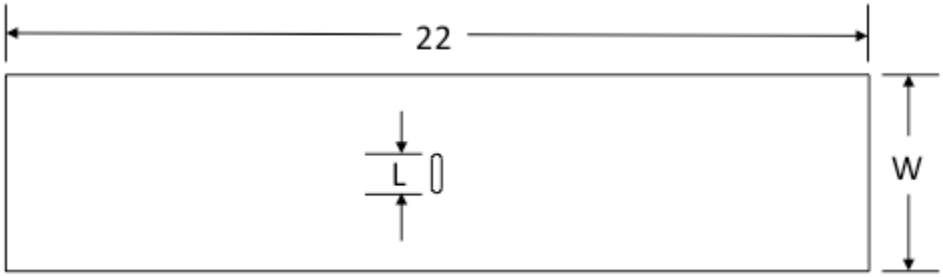

Figure 17. Specimen geometry (all dimensions in inches)

[1] W in figure 17 was 5 inches and 20 inches.

Figure 18. Four-point bending test fixture

During the tests, the laminates experienced large deflections before failure occurred. One consequence of large deflections involves anticlastic curvature effects. During pure bending of a plate, a radius of curvature R_x is formed in the principal bending direction, as shown in figure 19. The Poisson effect causes curvature of the plate in the transverse direction with radius R_y. The transverse curvature tends to move the fibers near the edge of the plate away from the principal axis of curvature causing them to go into tension. It also tends to move the fibers at the center of the plate closer to the principal axis of curvature causing them to go into compression. The combination of these two effects tends to flatten the plate in the transverse direction, causing it to bend into the shape of a cylinder. This, in turn, causes a transverse bending moment to develop except at the edges where the transverse moment must be zero. The severity of this effect is a function of the Searle parameter $b^2/(R_x t)$), where b is the plate width and t is the plate thickness [26, 27]. This effect was amplified in the present tests by applying the loads through relatively rigid bars in the test fixture. An FEA was performed on a plate without a notch. Figure 20 shows a contour plot of the bending moment per unit length along the longitudinal (principal bending) direction. As shown, the moment is not quite uniform in the center portion of the plate. Figure 21 shows a contour plot of the bending moment per unit length along the transverse direction. The maximum value of the transverse moment is approximately one-third that of the longitudinal moment. Also, the transverse moment is very nonuniformly distributed. Therefore, in the present tests, damage developed in advance of the notch tip into a nonuniform biaxial bending field. The degree of biaxiality is a function of plate thickness. In the tests, it was found that the far-field transverse strains were negligible (on average, less than 1% of the longitudinal strains) for all of the 20-ply laminates. The same was true for the 40-ply laminates with 4-inch notches. However, for the 40-ply laminates with 1-inch notches, the transverse strains were, on average, 13% of the longitudinal strains.

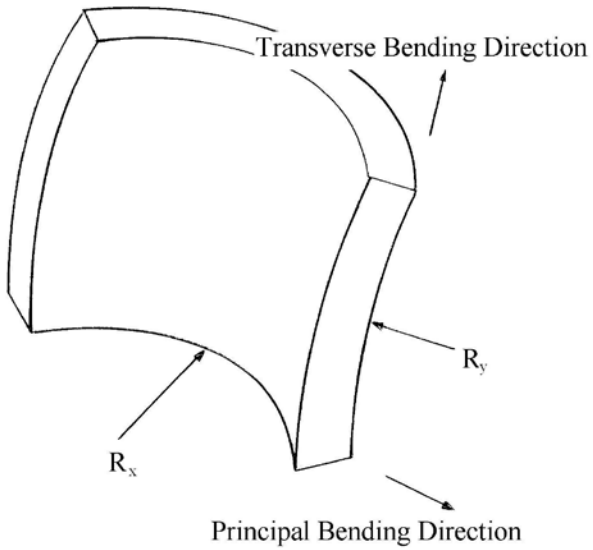

Figure 19. Anticlastic curvature effects with large deflections

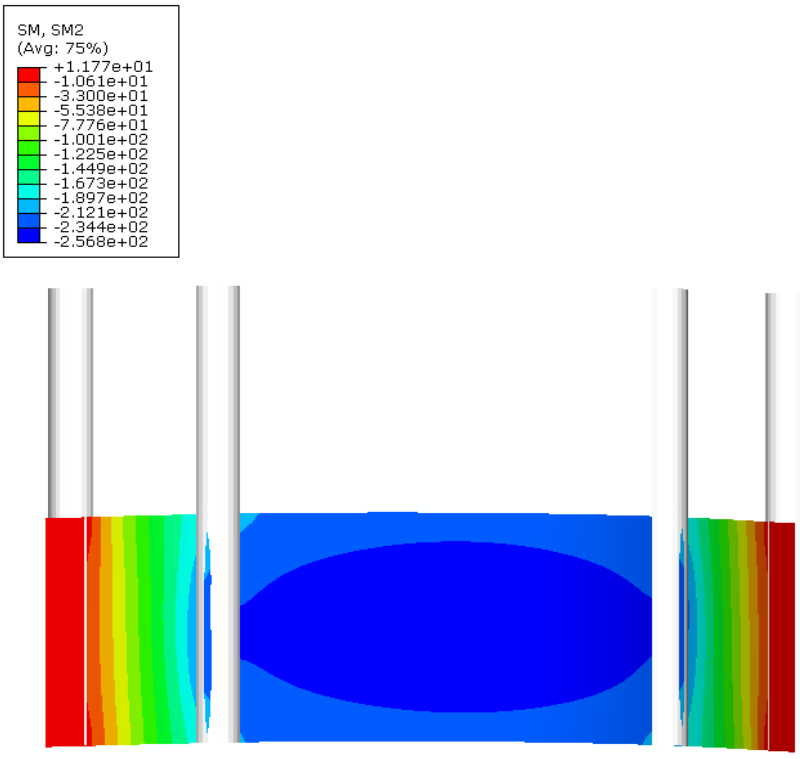

Figure 20. Bending moment per unit length in the longitudinal direction

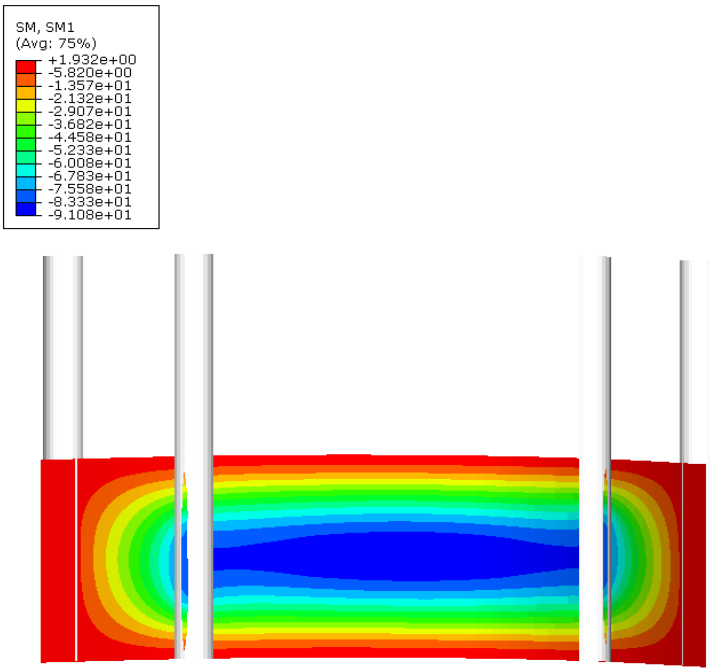

Figure 21. Bending moment per unit length in the transverse direction

4.2 FINITE ELEMENT MODELS

4.2.1 Progressive Damage Model

The goal of the progressive damage model is the ability to simulate the propagation of a notch in a composite laminate under out-of-plane bending. Williams [28] calculated the crack tip stress and displacement fields for a crack in an infinite isotropic plate under bending using classical plate theory. He found the usual square root singularity in stress at the crack tip, which can be expressed as

$$\sigma = \frac{k_1}{\sqrt{2r}} \frac{2z}{h} \tag{34}$$

where k_1 is the stress-intensity factor. Two studies [16 and 28] have been conducted to calculate stress-intensity factors for orthotropic materials under bending.

In a composite material, a zone of damage of considerable influence is known to develop in advance of the notch. This is the result of a combination of failure modes, including fiber breaking, matrix cracking, etc. Consequently, the usual fracture mechanics procedures that have worked successfully in metal structures do not work well for composites [29–31]. The simulation of damage progression in a composite is best accomplished with theories that incorporate principles from the field of damage mechanics. Several such theories [32–36] that treat damage development in the laminate as a whole rather than on a ply-by-ply basis have been successful in simulating notch growth under in-plane loading. In the case of bending, there is a nonuniform strain through the thickness of the laminate. A theory that treats damage progression at the ply level is needed for this case.

For progressive damage analysis, the model in ABAQUS for composite materials was used [37]. This model is based on the work of Matzenmiller, Lubliner, and Taylor [38]; Hashin and Rotem [39]; Hashin [40]; and Camanho and Davila [41]. It considers four different failure modes: (1) fiber rupture in tension; (2) fiber buckling and kinking in compression; (3) matrix cracking under transverse tension and shearing; and (4) matrix crushing under transverse compression and shearing. It uses concepts from the field of continuum damage mechanics. When damage occurs (e.g., microcracking, etc.), the effective load-carrying area of the material is considered to be reduced, and the concept of an effective stress is introduced to account for the area reduction:

$$\hat{\sigma} = \frac{\sigma}{1-d} \tag{35}$$

The quantity d is a damage variable that ranges from 0 (no damage) to 1 (development of a macrocrack). From this, an effective stress tensor is introduced as

$$\{\hat{\sigma}\} = [M]\{\sigma\} \tag{36}$$

where $\{\sigma\}$ is the usual two-dimensional stress in column-matrix form in principal material directions and M is a damage operator given as

$$[M] = \begin{bmatrix} \frac{1}{1-d_f} & 0 & 0 \\ 0 & \frac{1}{1-d_m} & \\ & & \frac{1}{1-d_s} \end{bmatrix} \tag{37}$$

where d_f, d_m, and d_s are damage variables characterizing fiber, matrix, and shear damage, respectively.

The constitutive relation for the material is affected by damage and results in a strain-softening response given by

$$\{\sigma\} = [C_d]\{\varepsilon\} \tag{38}$$

where $\{\varepsilon\}$ is the usual two-dimensional strain in column-matrix form and $[C_d]$ is the effective elasticity matrix given by

$$[C_d] = \frac{1}{D}\begin{bmatrix} (1-d_f)E_1 & (1-d_f)(1-d_m)\nu_{21}E_1 & 0 \\ (1-d_f)(1-d_m)\nu_{12}E_2 & (1-d_f)E_1 & 0 \\ 0 & 0 & (1-d_s)G_{12} \end{bmatrix} \tag{39}$$

where $D = 1-(1-d_f)(1-d_m)\upsilon_{12}\,\upsilon_{21}$ and E_1, E_2, G_{12}, υ_{12}, and υ_{21} are the usual orthotopic elastic constants.

The initiation of damage depends on which of the four failure modes is activated. The criteria for initiation use Hashin's theory and are governed by the following relations:

- Fiber tension $(\hat{\sigma}_{11} \geq 0)$:

$$\left(\frac{\hat{\sigma}_{11}}{X^T}\right)^2 + \alpha\left(\frac{\hat{\tau}_{12}}{S^L}\right)^2 = 1 \tag{40}$$

- Fiber compression $(\hat{\sigma}_{11} < 0)$:

$$\left(\frac{\hat{\sigma}_{11}}{X^C}\right)^2 = 1 \tag{41}$$

- Matrix tension $(\hat{\sigma}_{22} \geq 0)$:

$$\left(\frac{\hat{\sigma}_{22}}{Y^T}\right)^2 + \left(\frac{\hat{\tau}_{12}}{S^L}\right)^2 = 1 \tag{42}$$

- Matrix compression $(\hat{\sigma}_{22} < 0)$:

$$\left(\frac{\hat{\sigma}_{22}}{2S^T}\right)^2 + \left[\left(\frac{Y^C}{2S^T}\right)^2 - 1\right]\frac{\hat{\sigma}_{22}}{Y^C} + \left(\frac{\hat{\tau}_{12}}{S^L}\right)^2 = 1 \tag{43}$$

where X^T is the tensile strength in the fiber direction, X^C is the compressive strength in the fiber direction, Y^T is the tensile strength in the direction perpendicular to the fibers, Y^C is the compressive strength in the direction perpendicular to the fibers, S^L is the longitudinal shear strength, S^T is the transverse shear strength, and α is a coefficient that determines the contribution of the shear stress to the fiber tensile initiation criterion.

The incorporation of strain softening into an FEA usually results in calculations that are mesh sensitive. This occurs because, as the mesh is refined, there is a tendency for the damage zone to localize to a zero volume. This leads to a prediction of structural failure with zero energy dissipation, which is physically impossible. Several techniques have been proposed to address this issue. One of the simplest, which was pioneered by Hillerborg [42], is to use a stress-displacement law rather than a stress-strain law in the damaged material. The ABAQUS program accomplishes this by introducing a characteristic length L^c based on element size. From this, equivalent displacements and equivalent stresses are defined for the four modes of failure as follows.

- Fiber tension $(\hat{\sigma}_{11} \geq 0)$:

$$\delta_{eq}^{ft} = L^c \sqrt{\langle \varepsilon_{11} \rangle^2 + \alpha \varepsilon_{12}^2} \tag{44}$$

$$\sigma_{eq}^{ft} = \frac{\langle \sigma_{11} \rangle \langle \varepsilon_{11} \rangle + \alpha \tau_{12} \varepsilon_{12}}{\delta_{eq}^{ft} / L^c} \tag{45}$$

- Fiber compression $(\hat{\sigma}_{11} < 0)$:

$$\delta_{eq}^{fc} = L^c \langle -\varepsilon_{11} \rangle \tag{46}$$

$$\sigma_{eq}^{fc} = \langle -\sigma_{11} \rangle \tag{47}$$

- Matrix tension $(\hat{\sigma}_{22} \geq 0)$:

$$\delta_{eq}^{mt} = L^c \sqrt{\langle \varepsilon_{22} \rangle^2 + \varepsilon_{12}^2} \tag{48}$$

$$\sigma_{eq}^{mt} = \frac{\langle \sigma_{22} \rangle \langle \varepsilon_{22} \rangle + \tau_{12} \varepsilon_{12}}{\delta_{eq}^{mt} / L^c} \tag{49}$$

- Matrix compression $(\hat{\sigma}_{22} < 0)$:

$$\delta_{eq}^{mc} = L^c \sqrt{\langle -\varepsilon_{22} \rangle^2 + \varepsilon_{12}^2} \tag{50}$$

$$\sigma_{eq}^{mc} = \frac{\langle -\sigma_{22} \rangle \langle -\varepsilon_{22} \rangle + \tau_{12} \varepsilon_{12}}{\delta_{eq}^{mc} / L^c} \tag{51}$$

For a given failure mode, the stress-displacement law takes on the form shown in figure 22. The part of the curve with a positive slope (*OA*) follows the usual linear elastic relationship and can be expressed as

$$\sigma_{eq} = \frac{\delta_{eq}}{\delta_{eq}^{0}} \sigma_{eq}^{0} \tag{52}$$

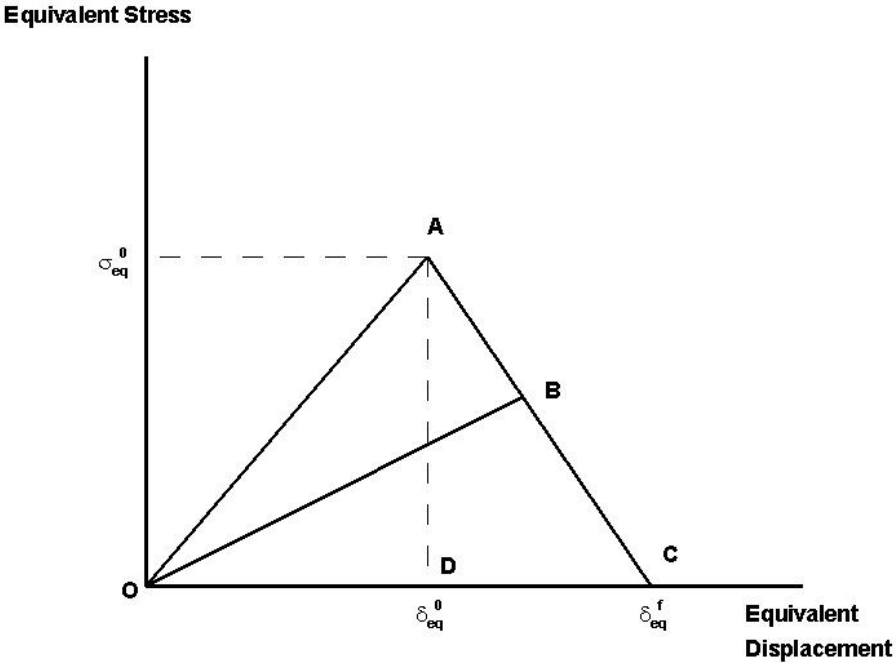

Figure 22. Stress-displacement constitutive law used in ABAQUS

The apex of the cure (*A*) represents the initiation of damage. Displacement beyond this point results in a decreasing stress. This part of the curve can be represented by

$$\sigma_{eq} = \frac{(\delta_{eq}^{f} - \delta_{eq})}{(\delta_{eq}^{f} - \delta_{eq}^{0})} \sigma_{eq}^{0} \tag{53}$$

After experiencing damage, the material unloads and reloads along line *OB*, which has a smaller slope than the original line *OA*. This reduced slope is accounted for using the damage variable *d* as

$$slopeOB = \frac{\sigma_{eq}^{0}}{\delta_{eq}^{0}} (1 - d) \tag{54}$$

Combining the last three equations with equation 35 gives the damage variable as

$$d = \frac{(\delta_{eq} - \delta_{eq}^{0})\delta_{eq}^{f}}{(\delta_{eq}^{f} - \delta_{eq}^{0})\delta_{eq}} \tag{55}$$

When running an analysis model in ABAQUS, the following parameters must be specified: X^T, X^C, Y^T, Y^C, S^L, S^T, α, and the dissipation energies (area under *OAC*) for each failure mode: G_{ft}, G_{fc}, G_{mt}, and G_{mc}.

4.2.2 Mesh Sensitivity Analysis

Finite element mesh sensitivity is known to be a problem with progressive damage models that incorporate strain softening to represent damage development (i.e., the solution does not converge with mesh refinement). To investigate this issue in the progressive damage model for composites in ABAQUS, analyses were performed on one test laminate (20 plies thick with 50% 0° plies) containing a 1-inch-long notch subjected to bending. Models were constructed using four different mesh densities. The coarsest mesh is shown in figure 23. This is a half-symmetry model. Although this assumption is not strictly correct because there is some weak coupling between bending and twisting, it was found to have a negligible effect on the results. A close-up view of the mesh near the notch tip is shown in figure 24, where it can be observed that there are 16 elements around the arc of the notch tip (total elements in the model = 750). Figure 25 shows a similar close-up view of the finest mesh that illustrates that there are 64 elements around the arc of the notch tip (total elements in the model = 6300). The failure moment per unit length was calculated for each mesh. A plot of failure moment per unit length versus the number of elements around the arc of the notch tip is shown in figure 26. The failure load increases with mesh refinement. This behavior occurs because the strength of an individual element depends on its size. To demonstrate this, an analysis was performed on a single square-shaped element subjected to a pure bending moment. Three different element edge lengths were considered: 0.05, 0.01, and 0.005 inch A plot of bending moment per unit length versus curvature for each element size is shown in figure 27. The maximum sustainable moment per unit length increases as the element size decreases.

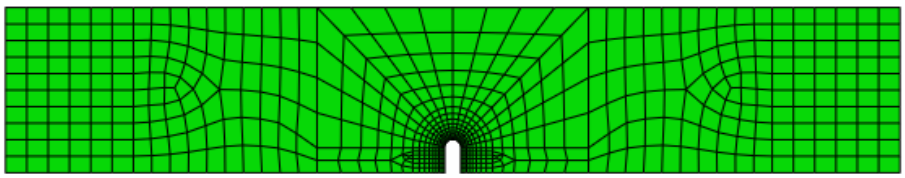

Figure 23. Coarsest finite element mesh for a laminate with a 1-inch-long notch

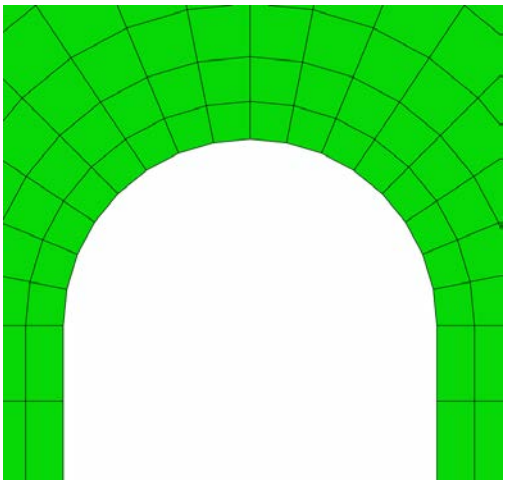

Figure 24. Close-up view of the notch tip for the coarsest mesh

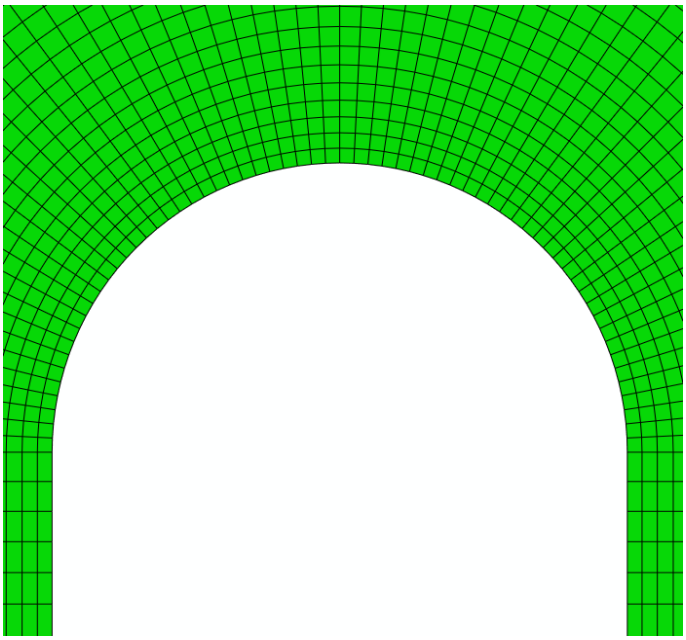

Figure 25. Close-up view of the notch tip for the finest mesh

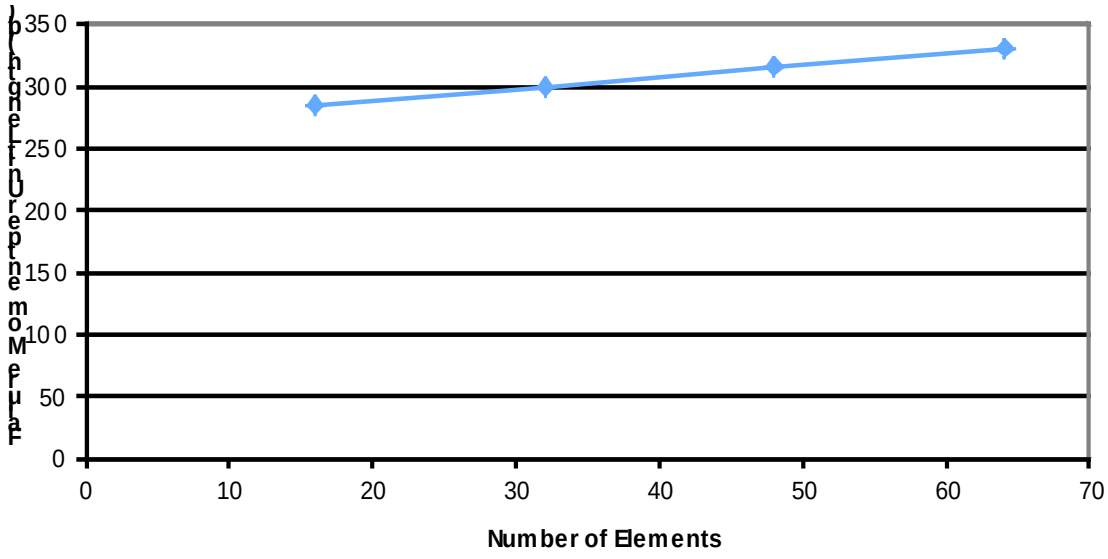

Figure 26. Failure moment per unit length vs the number of elements around the notch tip

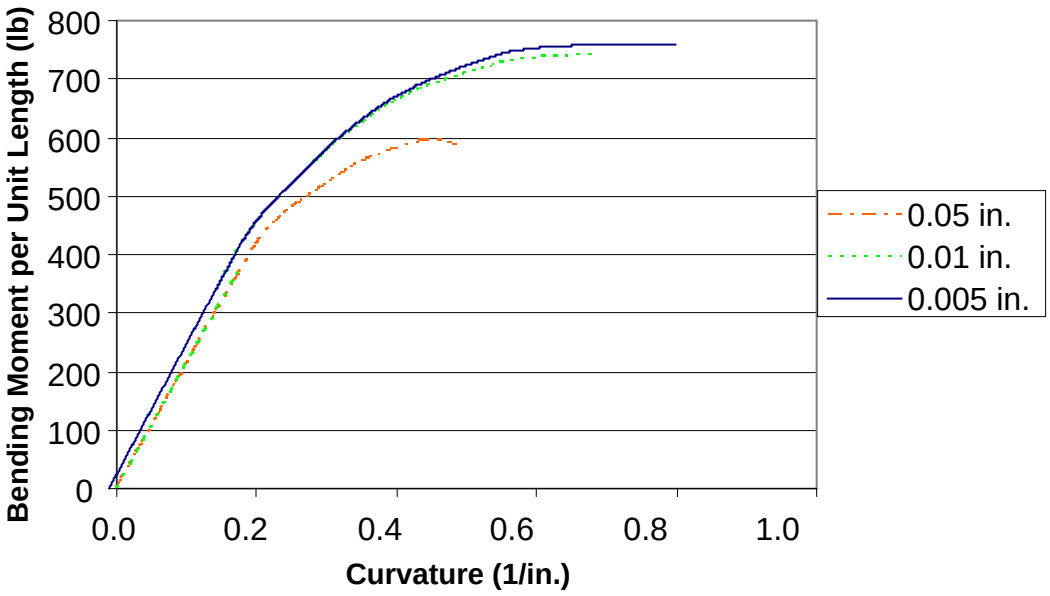

Figure 27. Bending moment per unit length vs curvature for elements with three different edge lengths

This behavior is linked to the method that ABAQUS uses to model damage progression described earlier. ABAQUS introduces a characteristic length, which is equal to the square root of the element area. If a single ply in simple tension is in the 1-direction, then the strain is $\varepsilon_{11} = \delta_{eq}/L$ (figure 22). For the simple tension case, $\sigma_{eq}^{o} = X$. The strain at the onset of damage is X/E_1, where E_1 is the elastic modulus in the 1-direction. The strain at complete failure (total loss of load-carrying capacity) is $\varepsilon_f = 2G_{Ic}/(XL)$. The behavior in compression is similar. A plot of the stress-strain curve for elements with edge lengths of 0.05 and 0.01 inch is shown in figure 28 for

compression loading in the 1-direction. As the element size decreases, the amount of strain softening after initiation of damage decreases. To see how this would affect a laminate under bending, consider a laminate with the following lay-up $(0/90/90/0/0/90/90/90/90/90)_s$. This simple lay-up was chosen so that almost all of the load would be carried by the 0° plies. Plots of moment per unit length versus curvature for two element sizes are shown in figure 29. The outside surface ply on the compression side would reach the damage initiation point first. The load-carrying capacity of this ply would be degraded with increasing strain according to the stress-strain curves shown in figure 28. Because the outside surface plies in the larger element would shed load more rapidly than those in the smaller element, the total load capacity of the larger element is less than the smaller element, as expected.

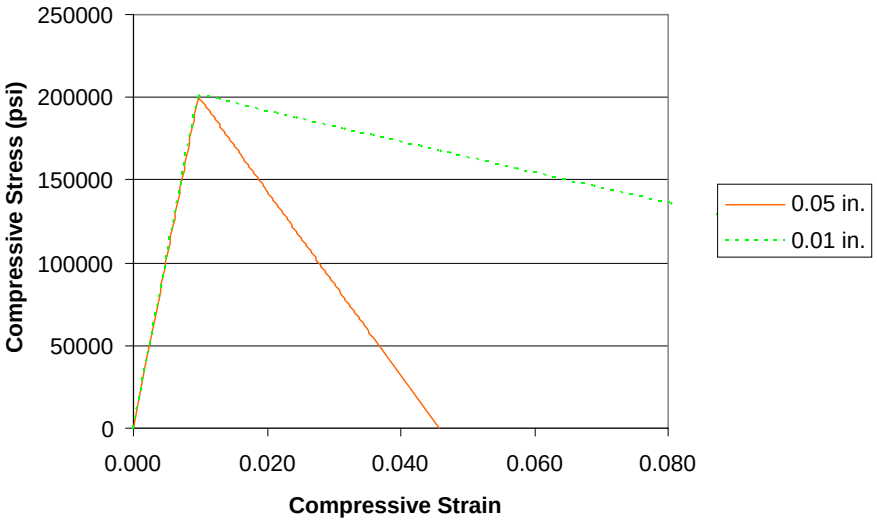

Figure 28. Stress-strain curves for a single ply modeled with elements with two different edge lengths

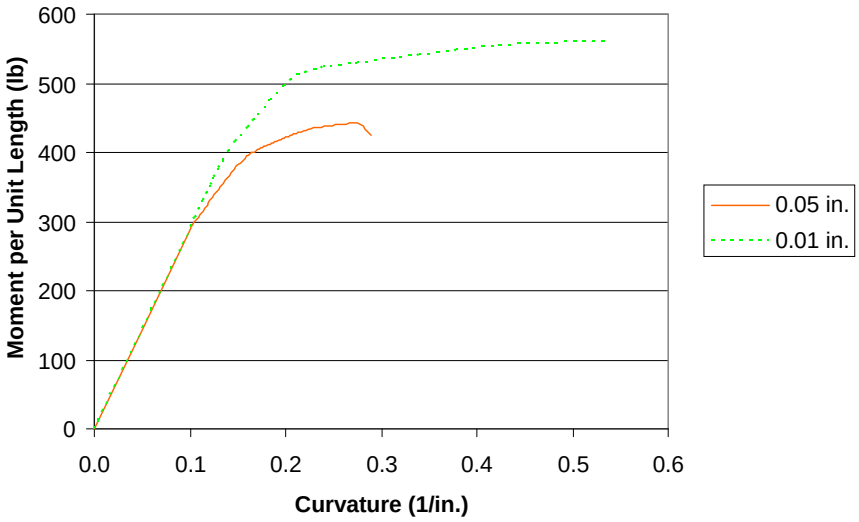

Figure 29. Bending moment per unit length vs curvature for elements with two different edge lengths for a laminate with a simple lay-up

The primary conclusion from this is that the analyst should account for the fact that the strength of an element is size dependent when creating a mesh. The usual practice of creating a graded mesh ranging from fine to course with distance from a stress concentration may be problematic. Elements of relatively equal size should be used in areas where damage is expected to develop. Fortunately, the mesh density appears to have a weak influence on failure load for this damage model.

4.2.3 Delamination Modeling

The delamination between plies was modeled using the Virtual Crack Closure Technique (VCCT) [43]. This technique uses the principles of linear elastic fracture mechanics and allows crack propagation when a critical value of the strain energy release rate is attained. The crack must propagate along a predefined path at the interface between elements. The strain energy release rate is calculated from the energy required to close the crack over one element length. Crack growth is assumed to occur when the following criterion is met

$$\frac{G_I}{G_{Ic}} + \frac{G_{II}}{G_{IIc}} + \frac{G_{III}}{G_{IIIc}} \tag{56}$$

where G_j is the strain energy release rate for mode j ($j = I, II, III$), and G_{jc} is the critical strain energy release rate for mode j. The critical strain energy release rate must be determined from interlaminar fracture tests.

4.2.4 Finite Element Models

Two finite element models were constructed—one that allowed delamination between plies and one that did not. The model that allowed delamination was composed of eight-node continuum shell elements stacked through the thickness of the laminate, as shown in figure 30, for a 1-inch-long notch. Only one-half of the plate was modeled. Although this symmetry assumption is not strictly valid because of some weak coupling between bending and twisting, it had negligible effect on the failure load. The interior interfaces between the element layers were allowed to debond according to the VCCT model. Various locations of the interfaces were explored to determine their effect on failure load, as described in the next section. The model that did not allow delamination was composed of a single layer of four-node conventional shell elements. Both models were constructed for laminates with a 4-inch-long notch (figure 31).

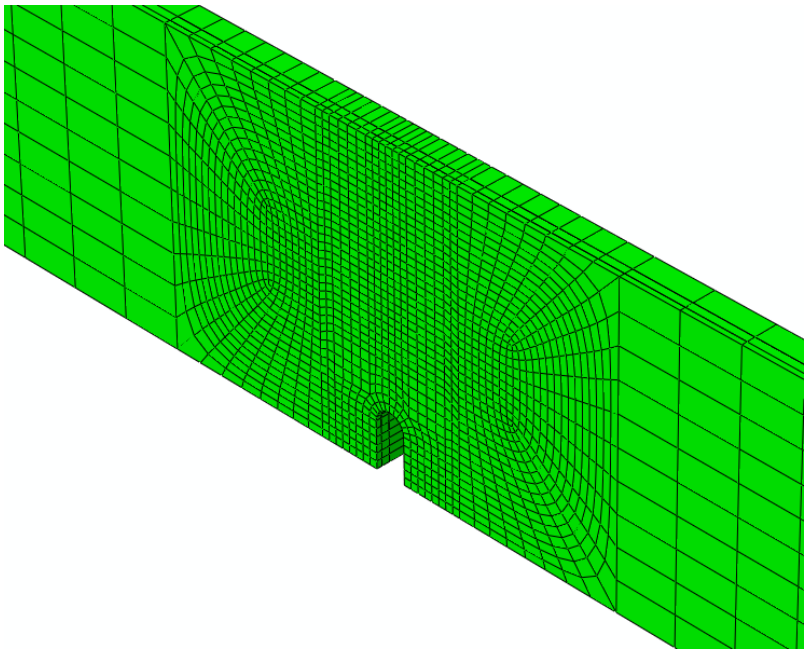

Figure 30. Half-Symmetry finite element model for laminates with a 1-inch notch

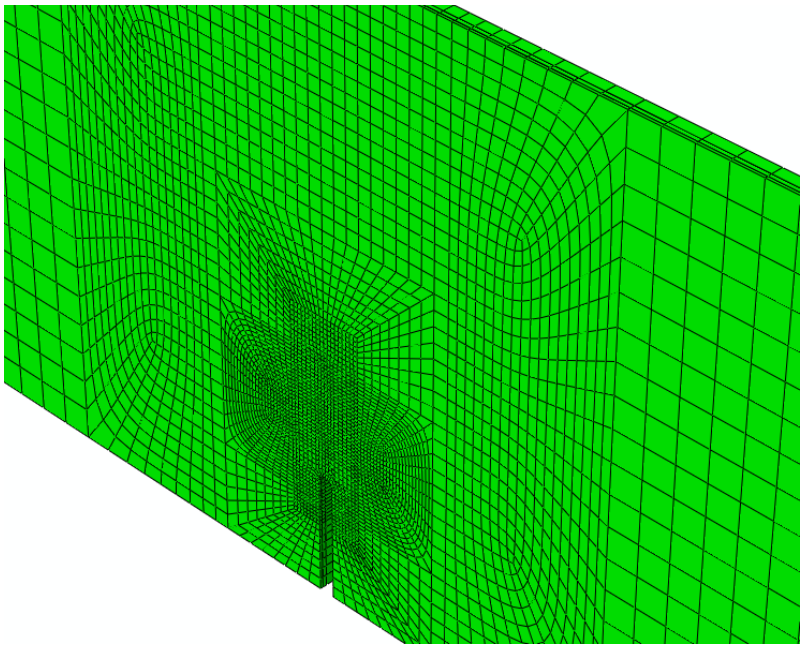

Figure 31. Half-symmetry finite element model for laminates with a 4-inch notch

4.3 TEST RESULTS AND DAMAGE ANALYSIS

During the four-point bending tests, the laminates experienced large deflections before failure. This is shown in figure 32, which shows the reaction forces between the laminate and the bars in the test fixture. The loads were normal to the surface of the laminate. As the laminate rotated during deflection, a significant horizontal component of force developed in addition to the

vertical component. The horizontal forces made a significant contribution to the bending moment experienced at the center portion of the laminate where the notch was located (note that the horizontal forces are, in general, not equal, resulting in a small axial load effect that was superposed on the bending moment at the center). Because the load cell in the test machine recorded only the vertical component of the load, it could not be used to determine the bending moment at the center. Therefore, it was necessary to determine the bending moment using strain gage output coupled with analysis results. Strain gages were mounted on the specimens at a point representing strain in the far field. A comparison of far-field strains on the compression and tension sides of the specimen from the test and from the theoretical model is shown in figure 33 for a 20-ply laminate with 50% 0° plies containing a 1-inch notch. The agreement between the test results and theoretical predictions was good with the exception that the theory predicted a slightly higher failure strain for this case. Considering all cases, the agreement between measured strain and predicted strain was generally good as load increased (the only disagreement was the load point at maximum strain). Therefore, some confidence exists that the model represents the response of the laminate for loads below the ultimate load. The analysis results were used to determine the test failure load in the following manner. It was assumed that the ultimate load is reached when the measured far-field strain peaks. At this strain, the response state of the model was checked. The far-field bending moment per unit length averaged over the width of the specimen was taken as the test failure load. Table 1 gives this load for each specimen.

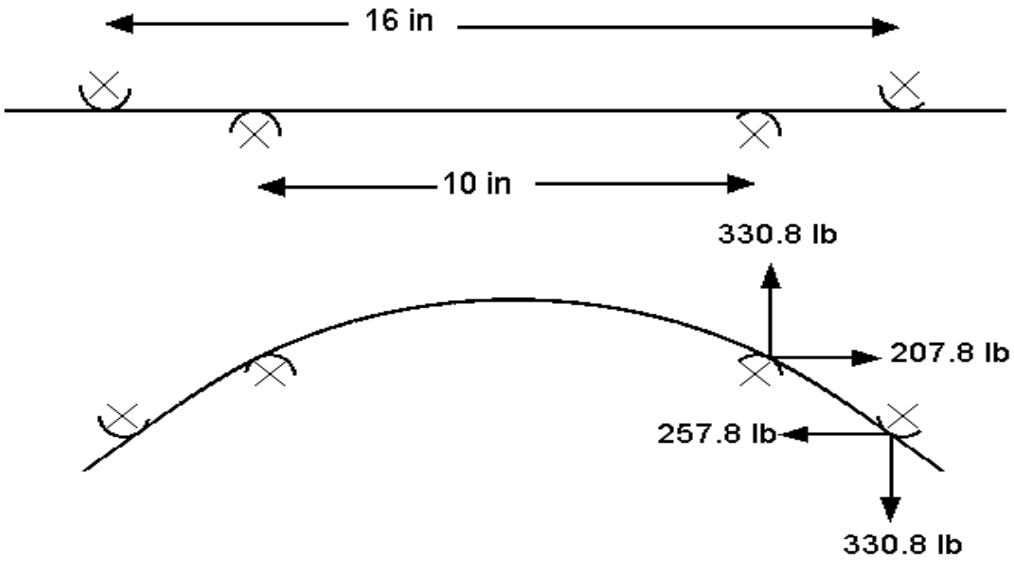

Figure 32. Applied loads with large deflection effects

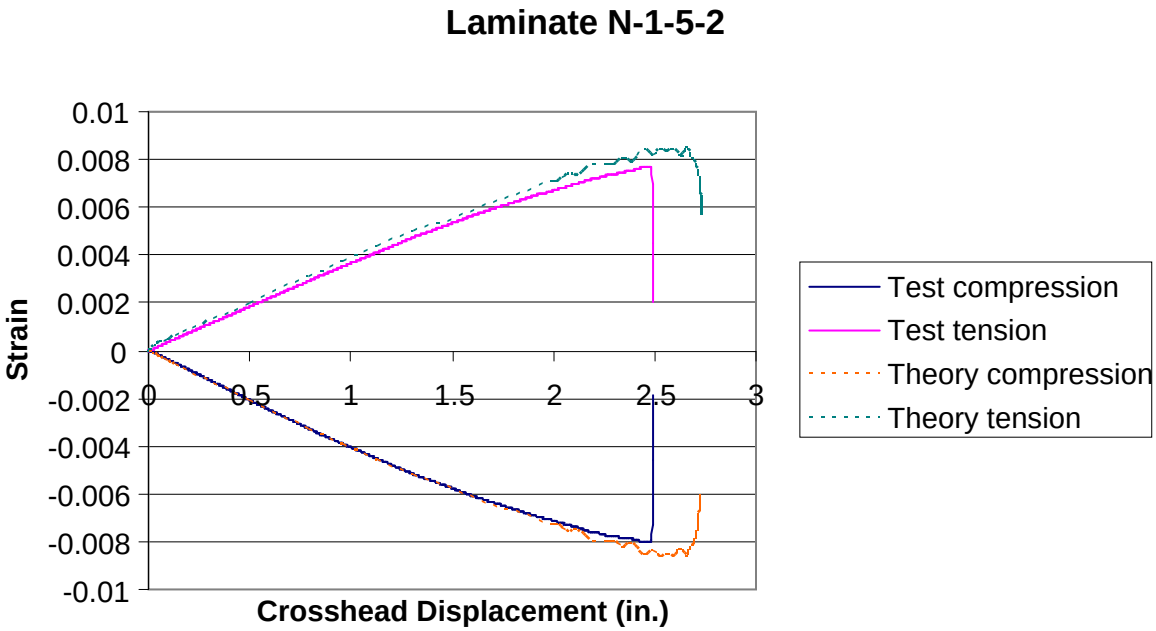

Figure 33. Far-field strain vs crosshead displacement

Table 1. Failure moment per unit length measured in the tests

Specimen	Percent 0° Plies	Number of Plies	Notch Length (inch)	Test Failure Moment (in-lb/inch)
f-1-5-1	10	20	1	193
f-1-5-2	10	20	1	173
p-1-5-1	30	20	1	186
p-1-5-2	30	20	1	200
p-1-5-3	30	20	1	192
n-1-5-1	50	20	1	231
n-1-5-2	50	20	1	246
n-1-5-3	50	20	1	260
fp-1-5-1	10	40	1	589
fp-1-5-2	10	40	1	615
fp-1-5-3	10	40	1	611
ar-1-5-1	30	40	1	735
ar-1-5-2	30	40	1	792
ar-1-5-3	30	40	1	693
an-1-5-1	50	40	1	919
an-1-5-2	50	40	1	916
an-1-5-3	50	40	1	884
f-4-20-1	10	20	4	209
f-4-20-3	10	20	4	208
p-4-20-1	30	20	4	191
p-4-20-2	30	20	4	198
p-4-20-3	30	20	4	175
n-4-20-1	50	20	4	233
n-4-20-2	50	20	4	224
n-4-20-3	50	20	4	226
fp-4-20-1	10	40	4	681
fp-4-20-2	10	40	4	605
fp-4-20-3	10	40	4	657
ar-4-20-1	30	40	4	641
ar-4-20-2	30	40	4	675
ar-4-20-3	30	40	4	688
an-4-20-1	50	40	4	989
an-4-20-2	50	40	4	943
an-4-20-3	50	40	4	931

During the tests, the 20-ply laminates exhibited negligible visible damage before failure, which was sudden and usually resulted in the laminate breaking into two pieces, as shown in figure 34. The 40-ply laminates exhibited a gradual progression of damage, which usually began with wrinkling of the outer ply on the compression side. This was followed by delamination at the outermost 0° ply and fracture of the plies between the outermost 0° ply and the surface. There was also some delamination between the second outermost 0° ply and the surface. The tension side of the laminate generally exhibited considerably less visible damage. This is shown in figure 35, which shows a close-up view of the laminate edge (the light-colored plies are the 0° plies). In some cases, it was observed that the plies between the outermost 0° ply and the surface buckled before fracturing, as shown in figure 36(a). This phenomenon was captured by the model, as shown in figure 36(b).

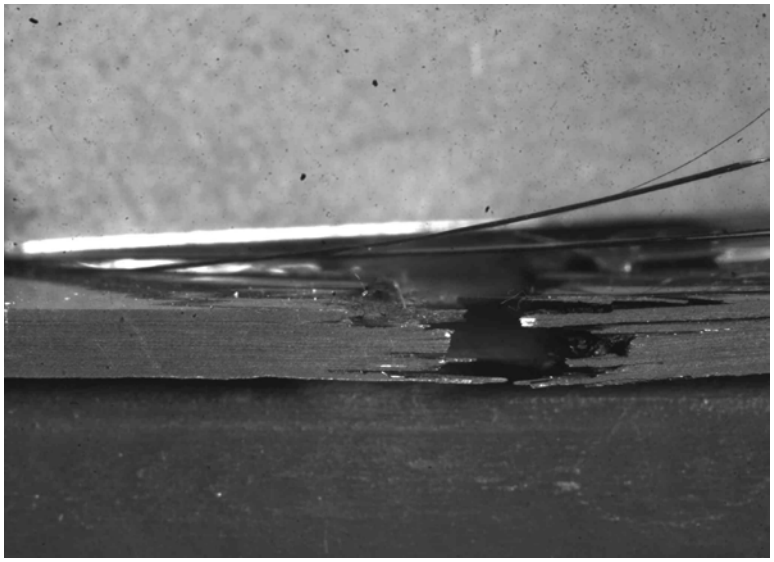

Figure 34. Fracture of a 20-ply laminate

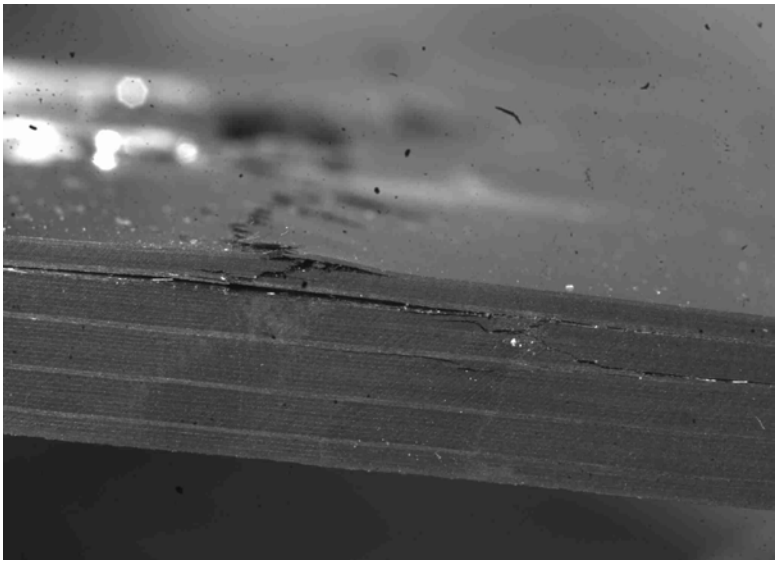

Figure 35. Delamination at the 0° plies (lighter-colored plies)

(a) Test

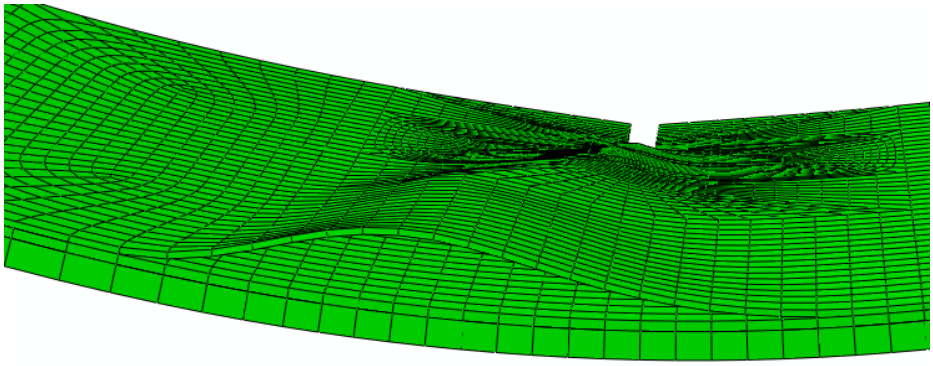

(b) Model

Figure 36. Postdelamination buckling

The first calculations were performed using the models with no delamination interfaces, as described in the previous section. For the 20-ply laminate, model results for the six cases examined varied from experiment, ranging from 11.5% lower to 9.5% higher, with an average difference of 2.9% lower. For the 40-ply laminate, model results for the six cases examined varied from experiment, ranging from 0.1% lower to 28.4% higher, with an average difference of 16.9% higher. These results are shown in figures 37–40.

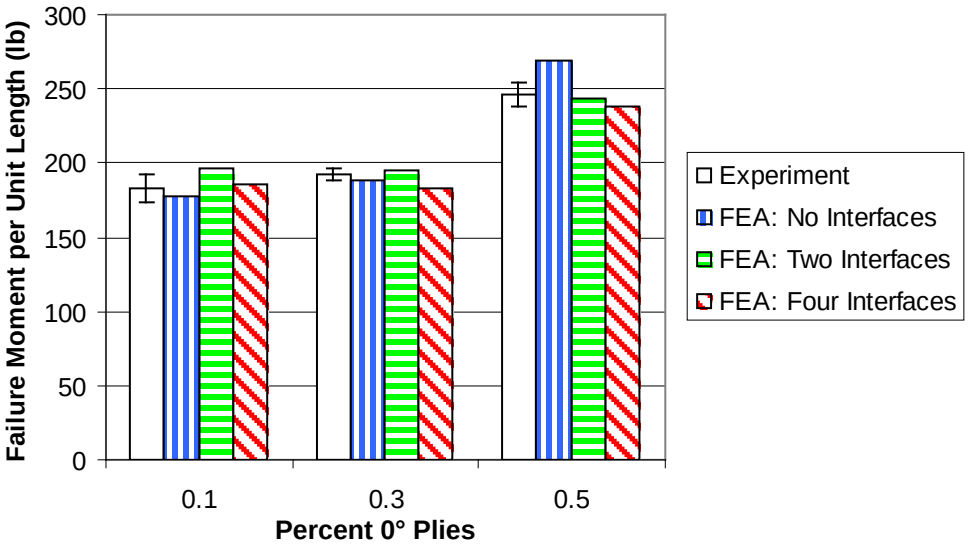

Figure 37. Comparison of test results and model predictions of failure moment per unit length for 20-ply laminates with a 1-inch-long notch

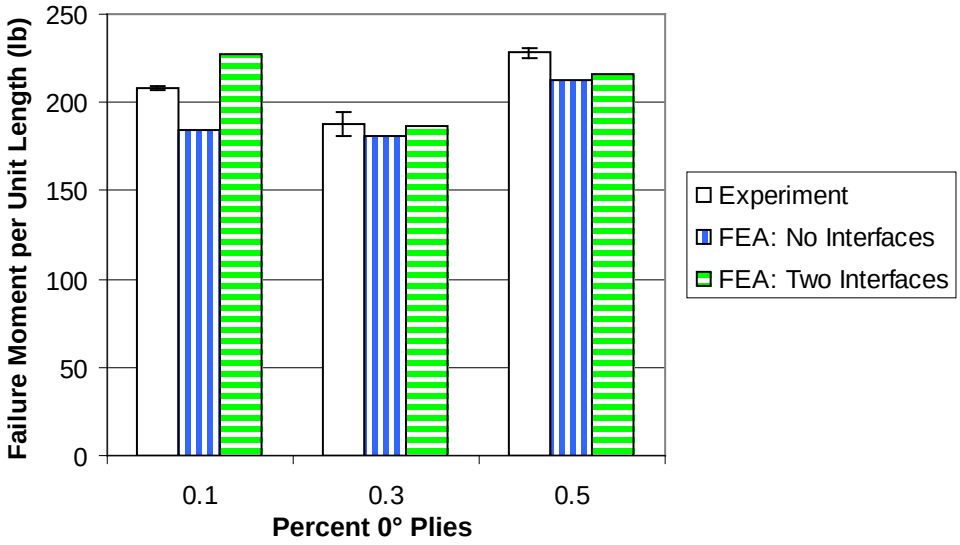

Figure 38. Comparison of test results and model predictions of failure moment per unit length for 20-ply laminates with a 4-inch-long notch

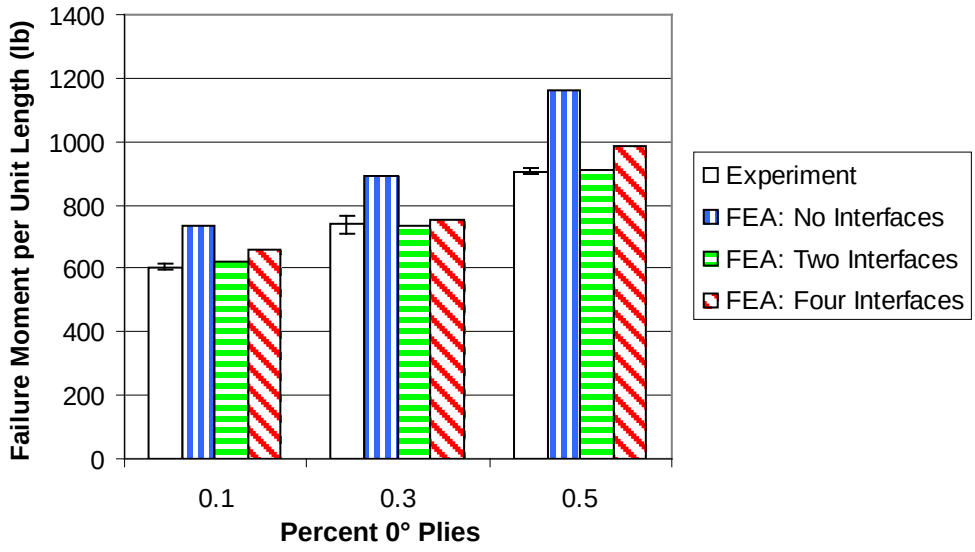

Figure 39. Comparison of test results and model predictions of failure moment per unit length for 40-ply laminates with a 1-inch-long notch

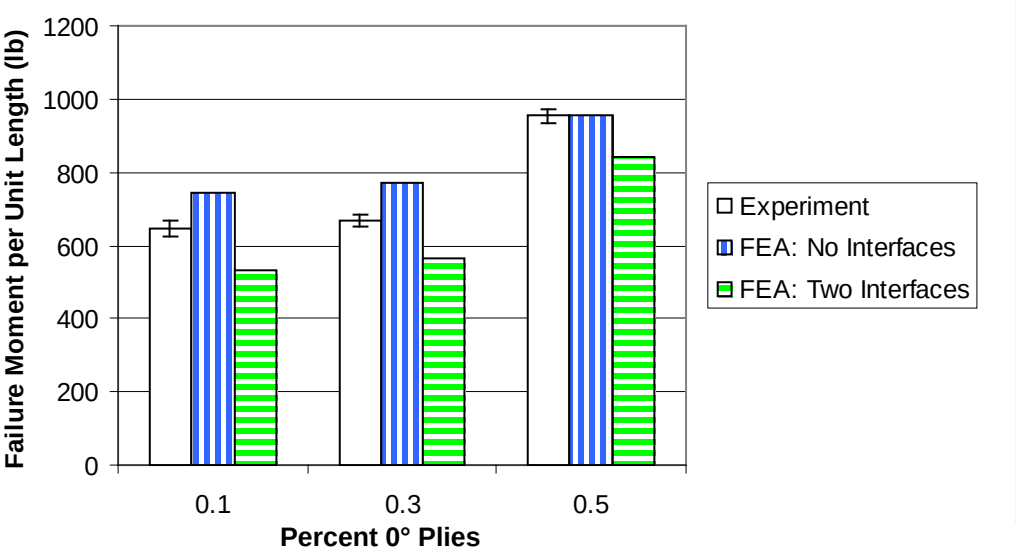

Figure 40. Comparison of test results and model predictions of failure moment per unit length for 40-ply laminates with a 4-inch-long notch

Experiments showed that the thicker, 40-ply laminates experienced delamination during fracture, allowing plies between the delamination and the surface to buckle outward. This caused a redistribution of the stress that led to further delamination and fracturing of additional plies. Because the progressive damage models used considered the plies to be perfectly bonded (i.e., no delamination interfaces existed in the model), this buckling failure mechanism was not replicated in the FEA results.

To more accurately model the laminate fracture, two delamination interfaces were added to the 40-ply laminated models. Two interfaces were also added to the 20-ply laminates to determine their effect. Interfaces were placed below (away from the compression surface) the outermost

compression-side 0° ply and below the second outermost 0° ply. These locations corresponded to where delamination was observed in the experiments.

As expected, based on the observed failure modes from the experiments, the addition of these interfaces to the models had a small effect on the calculated failure loads for the 20-ply laminates and a much greater effect for the 40-ply laminates. For the 20-ply laminate, analysis results, based on the six cases examined, varied from the experiment, ranging from 5.3%–9.1%, with an average difference of 1.7% compared to 2.9% with no interfaces. For the 40-ply laminate, the model results with interfaces varied from experiment, ranging from 18.1% lower to 3.0% higher, with an average difference of 6.7% lower compared to 16.9% lower with no interfaces. These results are also shown in figures 37–40.

To better understand the effect of delamination on the model, additional interfaces were added. In addition to interfaces below the outermost and second outermost 0° plies, interfaces were placed below the outermost ply and above the outermost 0° ply, for a total of four interfaces. The 20-ply, 10% 0° ply laminate was one exception. Only one 0° ply existed on the compression side, so only three interfaces were created. In addition, due to the excessively long run times associated with the 4-inch notch laminates, only 1-inch laminates were included in this aspect of the study.

In general, the additional delamination interfaces had a negligible effect on the calculated fracture loads. For the 20-ply laminates with 1-inch notches, the difference between the experimentally measured and the model-predicted failure loads varied from an average of 1.5% (model higher) with no interfaces, 2.4% (model higher) with two interfaces, to -2.4% (model lower) with four (or three as described above) interfaces. For the 40-ply laminates with 1-inch notches, the differences varied an average of 23.5% (model higher) with no interfaces, 1.7% (model higher) with two interfaces, and 6.4% (model higher) with four interfaces. These results are also shown in figures 37–40 and are summarized in table 2.

Table 2. Comparison of failure moment per unit length from the test and from the model

Number of Plies	Notch Length (inch)	0° Plies (%)	FEA: Difference From Experiment		
			No Interfaces (%)	Two Interfaces (%)	Four Interfaces (%)
20	1	10	-2.7	7.1	1.7%
		30	-2.2	1.3	-5.4
		50	9.5	-1.2	-3.4
	4	10	-11.5	9.1	
		30	-3.7	-0.5	
		50	-6.4	-5.3	
40	1	10	21.2	3.0	8.7
		30	20.8	-0.9	1.8
		50	28.4	3.0	8.7
	4	10	14.8	-18.1	
		30	15.7	-15.6	
		50	0.1	-11.5	

5. TASK 5: SENSITIVITY ANALYSIS OF DAMAGE PARAMETERS

The progressive damage model in ABAQUS requires that ply strength properties (damage initiation) and ply dissipation energies (damage evolution) be specified (see section 4.2). These properties are generally determined through coupon tests and analysis, and in many cases, the uncertainty in these values is high. The objective of this task was to determine the sensitivity of the laminate failure moment per unit length to these parameters. This was accomplished by performing a systematic series of numerical experiments using the design of experiments methodology.

The material selected for this study was a carbon fiber/epoxy matrix composite with the properties given in table 3 [44]. The damage parameter properties are material properties associated with the Hashin progressive damage model described in section 4.2.1. The laminate that was studied had the following lay-up: $[-45/0/0/45/90/-45/0/0/45/90]_s$. This laminate has bending stiffness properties with D_{11} = 3473 in-lb and D_{22} = 1602 in-lb. The orthotropy is such that the stiff direction has approximately double the stiffness in the soft direction. The sensitivity study was performed for both the stiff and soft directions of the laminate with a 1-inch-long notch under four-point bending.

Table 3. Selected Carbon Fiber/Epoxy Matrix Composite Properties

Elastic Properties	Value
E_1 (Mpsi)	21.3
E_2 (Mpsi)	1.65
ν_{12}	0.3
G_{12} (Mpsi)	0.885
G_{13} (Mpsi)	0.885
G_{23} (Mpsi)	0.565
Damage Parameter Properties	Value
X_T (psi)	251,000
X_C (psi)	200,000
Y_T (psi)	9,645
Y_C (psi)	30,000
S_L (psi)	15,880
S_T (psi)	11,300
G_{FT} (lb/in)	513
G_{FC} (lb/in)	447
G_{MT} (lb/in)	5.71
G_{MC} (lb/in)	25

Laminate failure analyses were performed for each of the ten damage parameters at a low and a high value, with the low value 20% below the nominal value and the high value 20% above the nominal value. A complete 2^{10} factorial design for this case would have required 1024 computer runs, which was not practical. Therefore, a fractional factorial design with 2^{10-6} (=16) runs was performed, which results in a Resolution III design in which no main (single factor) effects are aliased (confounded) with any other main effect, but main effects are aliased with two factor interactions, and two factor interactions may be aliased with each other [45]. Table 4 shows the labels given to each of the damage parameters. Table 4 also gives a list of the two factor interactions that are aliased with each main effect. Aliased factors greater than two were omitted from this table because it is assumed that they are negligible in comparison. Table 5 shows the experimental design matrix, which gives the magnitudes of the factors for each computer run, where -1 indicates a low value of the parameter and +1 indicates a high value of the parameter. The effect of a factor is defined as the difference between the average response at the low level of the factor and the average response at the high level of the factor.

Table 4. Factor labels for damage parameters and aliases

Damage Parameter	Factor Label	Two Factor Aliases
X_T	A	FJ and BK
X_C	B	GJ and AK
Y_T	C	HJ and EK
Y_C	D	EJ and HK
S_L	E	DJ and CK
S_T	F	AJ and GK
G_{FT}	G	BJ and FK
G_{FC}	H	GJ and DK
G_{MT}	J	DE, AF, BG, and CH
G_{MC}	K	AB, CE, FG, and DH

Table 5. Factor magnitudes for each computer run

Run	A	B	C	D	E	F	G	H	J	K
1	-1	-1	-1	-1	-1	-1	-1	-1	1	1
2	1	-1	-1	-1	1	-1	1	1	-1	-1
3	-1	1	-1	-1	1	1	-1	1	-1	-1
4	1	1	-1	-1	-1	1	1	-1	1	1
5	-1	-1	1	-1	1	1	1	-1	-1	1
6	1	-1	1	-1	-1	1	-1	1	1	-1
7	-1	1	1	-1	-1	-1	1	1	1	-1
8	1	1	1	-1	1	-1	-1	-1	-1	1
9	-1	-1	-1	1	-1	1	1	1	-1	1
10	1	-1	-1	1	1	1	-1	-1	1	-1
11	-1	1	-1	1	1	-1	1	-1	1	-1
12	1	1	-1	1	-1	-1	-1	1	-1	1
13	-1	-1	1	1	1	-1	-1	1	1	1
14	1	-1	1	1	-1	-1	1	-1	-1	-1
15	-1	1	1	1	-1	1	-1	-1	-1	-1
16	1	1	1	1	1	1	1	1	1	1

A Pareto plot of the main effects (which represents the magnitude of the effect of a particular parameter on the laminate bending strength) is shown in figure 41 for the stiff direction of the laminate. It is clear from this plot that the four-ply damage parameters in the fiber direction have a much greater influence on failure moment than any of the other damage parameters. This is also shown in figure 42, which shows a normal quantile-quantile plot [46] of the effects of the damage parameters. Insignificant effects tend to fall along a straight line on this type of plot, but significant effects are well removed from the line. Again, the four-ply damage parameters in the fiber direction stand out as being the significant ones.

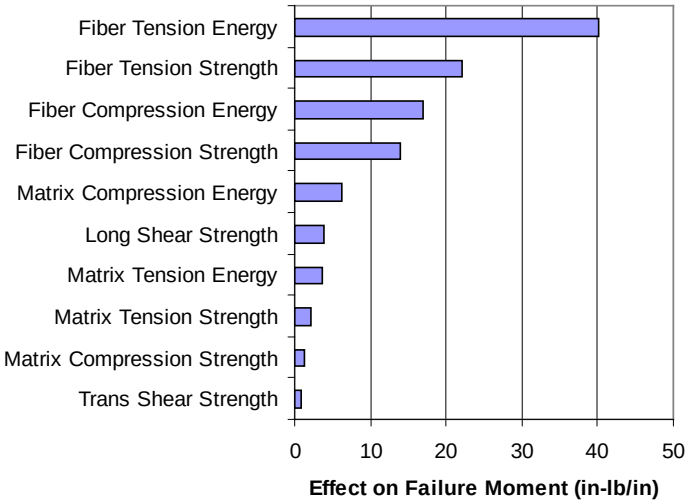

Figure 41. Pareto plot of the damage parameter effects for the stiff direction of the laminate

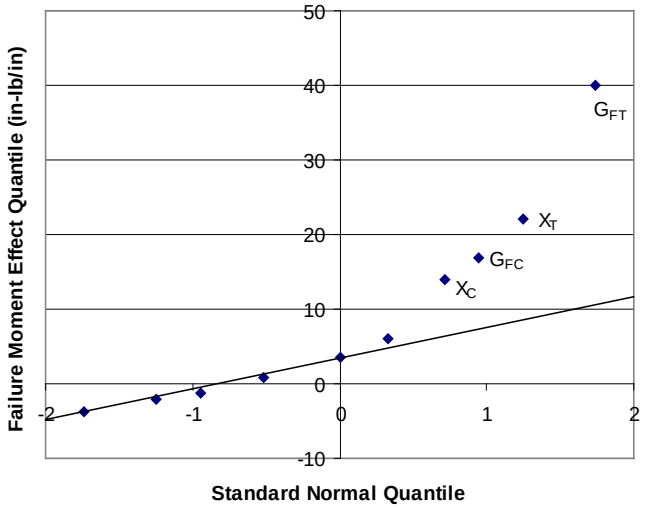

Figure 42. Normal quantile-quantile plot of the damage parameter effects on the failure moment for the stiff direction of the laminate

To get a more detailed comparison of the four largest effects (the damage parameters in the fiber direction), all damage parameters were set to their nominal values, and calculations were performed varying one factor at a time from a low value (20% below the nominal value) to a high value (20% above the nominal value). These results are shown in figure 43, which gives a plot of failure moment (normalized by dividing by the failure moment when all damage parameters are at their nominal values) versus a damage parameter (normalized by dividing it by its nominal value). It is evident that the effect of the damage parameters on the failure moment per unit length is generally nonlinear. The effect of the tension energy is almost linear. The effects of the tension strength and compression strength have decreasing slopes with increasing factor values. The effect of the compression energy has an increasing slope with an increasing

factor value. It should also be noted that a ±20% change in any of the damage parameter values causes a change in failure moment that is less than ±8%.

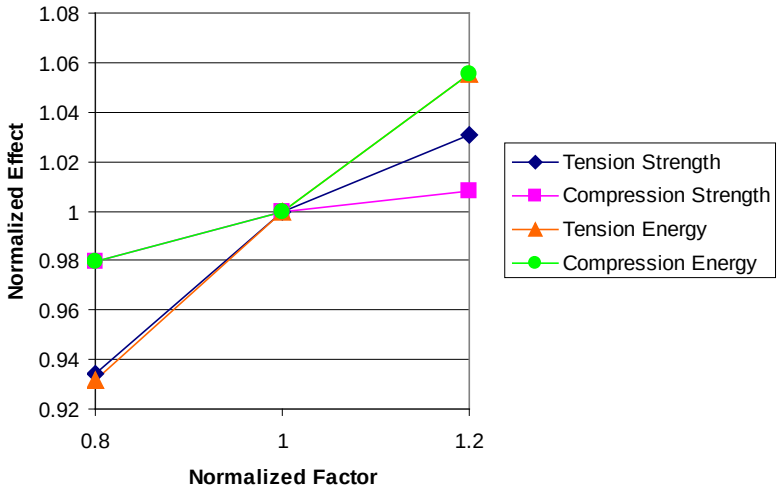

Figure 43. Normalized plot of the damage parameter effects on the failure moment per unit length for the stiff direction of the laminate

These calculations were repeated for the soft direction of the laminate. A Pareto plot of the main effects is shown in figure 44 for this case. As in the previous case, the four-ply damage parameters in the fiber direction had a much greater influence on failure moment than any of the other damage parameters. The normal quantile-quantile plot (figure 45) provides a similar conclusion. The effects of varying the four dominant parameters one at a time is shown in figure 46. In this case, all the effects have decreasing slopes with increasing factor values. Also, a ±20% change in any of the damage parameter values causes a change in failure moment that is less than ±6%.

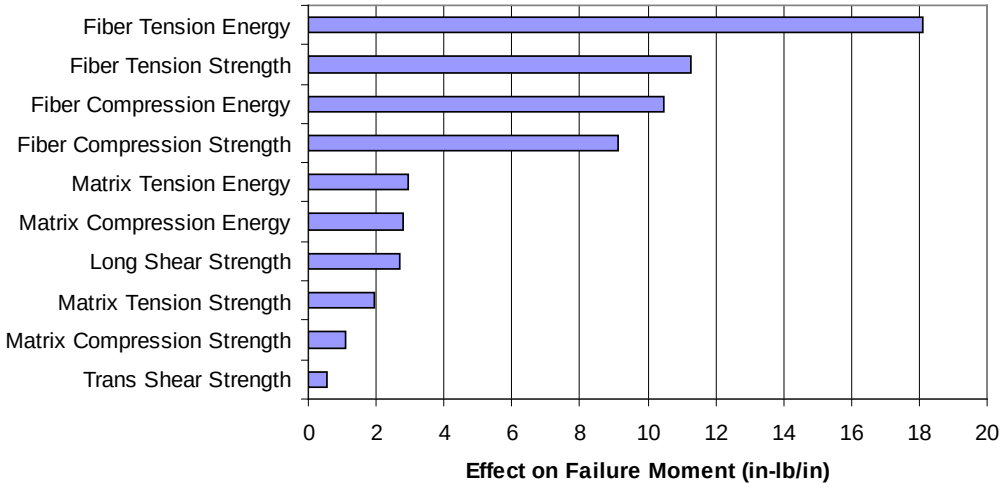

Figure 44. Pareto Plot of the damage parameter effects on the failure moment per unit length for the soft direction of the laminate

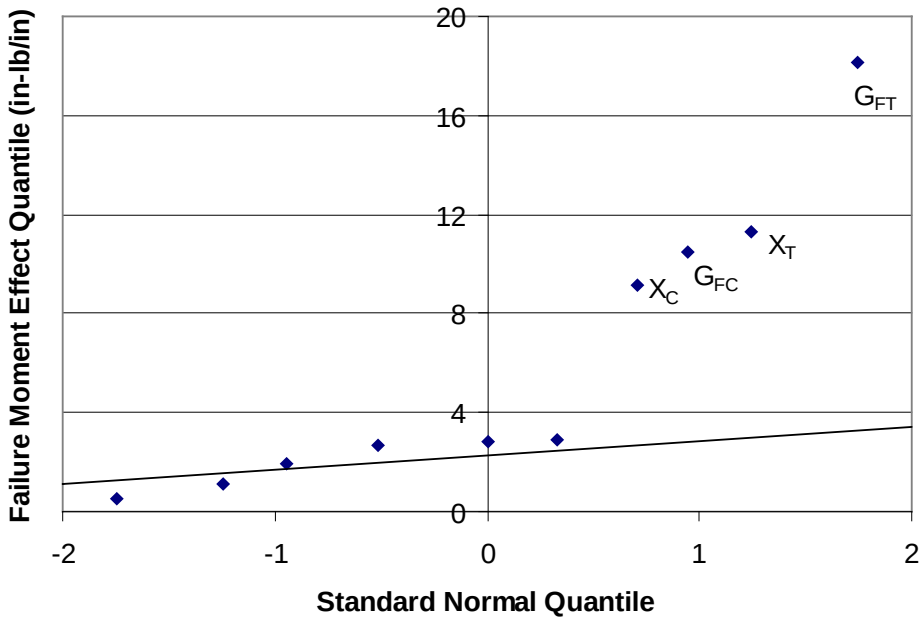

Figure 45. Normal quantile-quantile plot of the damage parameter effects on the failure moment per unit length for the soft direction of the laminate

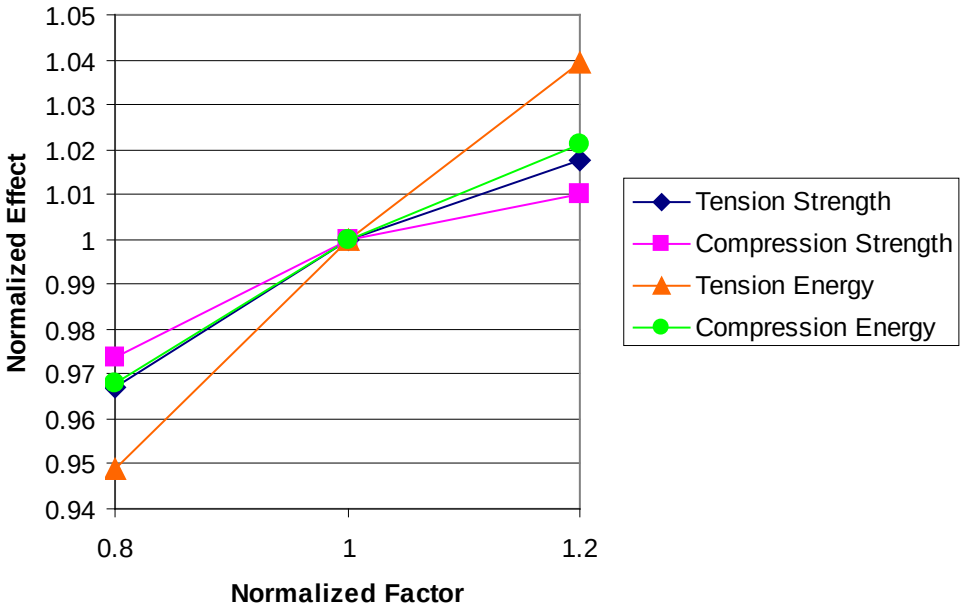

Figure 46. Normalized plot of the damage parameter effects on the failure moment per unit length for the soft direction of the laminate

The overall conclusion from these results is that the failure of notched laminates under bending is dominated by the ply properties in the fiber direction. Also, large changes in these properties (±20%) tended to produce small changes in failure load (<±7%). The relatively low sensitivity of failure load to these properties is a desirable outcome from a design perspective because it indicates a progressive damage analysis will not require highly accurate values of these

properties to be determined experimentally. These conclusions are valid only for thin laminates where delamination does not appear to have an important effect.

Because failure load is defined in this report as the maximum load carried by the panel, the maximum load consistently occurred after some damage had propagated. Therefore, the magnitude of the maximum load is a function of when damage initiates and when it propagates. Damage initiation, as shown in equations 40–43, depends on the six strength parameters. Damage propagation, as described in section 4.2.1, depends on the four energy parameters. The inclusion of a number of damage parameters and their interactions leads to failure load not being a simple function of the fiber strength alone. However, damage initiation has a one-to-one correlation to fiber strength.

6. CONCLUSIONS

The broad objective of this research was to determine the failure modes of notched laminates under bending and to evaluate the capability of some currently existing models to predict failures. A number of aspects of this problem were studied that resulted in the following conclusions:

- The elastic strain concentration factor near the notch is influenced by transverse shear effects, and these should be included in finite element models. Three-dimensional, free-edge effects are also evident, but dissipate rapidly with distance from the edge.
- Simple semi-empirical failure criteria, which have been useful for in-plane loading, do not appear to be an effective tool for using small notch data to predict failure for laminates with larger notches under bending.
- Failure progression in thin laminates appears to be different from that in thick laminates. Thin laminates exhibit negligible visible damage before failure, which is usually sudden and results in the laminate breaking into two pieces. Thick laminates exhibit a gradual progression of damage, which is usually confined to the compression side of the laminate. Also, delamination, followed by buckling of the plies between the delamination site and the surface on the compression side of the laminate, is an important failure mechanism for thick laminates.
- The progressive damage model for composite materials in the ABAQUS® program shows promise in its ability to predict failure in notched laminates under bending, including modeling complex delamination/buckling response.
- The failure load for notched laminates under bending is predominantly controlled by the ply properties in the fiber direction and is not very sensitive to changes in these properties. This conclusion may not be valid for failure initiation. These conclusions are valid only for thin laminates where delamination does not appear to have an important effect.
- Failure load predictions, with delamination interfaces present, for the 4-inch-long notch cases, particularly the 40-ply specimens, tended to be less accurate and lower than for the 1-inch-long notch cases. A possible cause of this behavior may be related to the values of ply delamination fracture toughness used in the models. It is common for the resistance to fracture to increase with growing crack size. This phenomena is manifested in the composite specimens used in this work as a crack initiation value of fracture toughness

and a crack propagation value of fracture toughness. To date, the work in this study has exclusively used the initiation toughness. Given that the initiation value is less than the propagation value and that the 4-inch cases have more area for delamination than the 1-inch cases, this may be the cause of the low predicted values. The next phase of this project is intended to explore the impact of incorporating propagating toughness values in the model as appropriate.

7. REFERENCES

1. Bradshaw, R.D. and Pang, S.S., "Failure Analysis of Composite Laminated Plates With Circular Holes Under Bending," *American Society of Mechanical Engineers, Petroleum Division (Publication) PD, V 37, Composite Material Technology*, 1991, pp. 125–135.

2. Shuart, M.J. and Prasad, C.B., "Analysis and Experiments for Composite Laminates With Holes and Subjected to Four-Point Bending," *AIAA/ASME/ASCE/AHS Structures, Structural Dynamics, and Materials Conference*, Long Beach, California, 1990, pp. 748–758.

3. Prasad, C.B., Shuart, M.J., Bains, N.J., and Rouse, M., "Effects of Cutouts on the Behavior of Symmetric Composite Laminates Subjected to Bending and Twisting Loads," NASA Report N95-28844, 1993.

4. Jones, D.L. and Subramonian, N., "An Analytical and Experimental Study of the Plate Tearing Mode of Fracture," *Engineering Fracture Mechanics*, Vol. 17, 1983, pp. 47–62.

5. Goodier, J.N., "The Influence of Circular and Elliptical Holes on the Transverse Flexure of Plates," *Philosophical Magazine*, Vol. 22, 1936, pp. 69–80.

6. Reissner, E., "The Effect of Transverse Shear Deformation on the Bending of Elastic Plates," *Journal of Applied Mechanics*, Vol. 67, 1945, pp. A69–A77.

7. Alblas, J.B., "Theorie van de Driedimensionale Spanningstoestand in een Doorboorde Plaat," Dissertation, Delft, Netherlands, 1957.

8. Lee, C.W., "Bending and Twisting of Thick Plates With a Circular Hole," *Journal of the Franklin Institute*, Vol. 285, 1968, pp. 377–385.

9. Reissner, E., "On Transverse Bending of Plates, Including the Effect of Transverse Shear Deformation," *International Journal of Solids and Structures*, Vol. 11, 1975, pp. 569–573.

10. Naghdi, P.M., "The Effect of Elliptic Holes on the Bending of Thick Plates," *Journal of Applied Mechanics*, Vol. 22, 1955, pp. 89–94.

11. Lekhnitskii, S.G., *Anisotropic Plates*, Gordon & Breach, New York, New York, 1968, pp. 403–410.

12. Prasad, C.B. and Shuart, M.J., "Moment Distributions Around Holes in Symmetric Composite Laminates Subjected to Bending Moments," *AIAA Journal*, Vol. 28, 1990, pp. 877–882.

13. Paul, T.K. and Rao, K.M., "Stress Analysis Around Circular Holes in FRP Laminates Under Transverse Load," *Computers & Structures*, Vol. 33, 1989, pp. 929–937.

14. Paul, T.K. and Rao, K.M., "Stress Analysis Around an Elliptical Hole in Thick FRP Laminates Under Transverse Loading," *Computers & Structures*, Vol. 35, 1990, pp. 553–561.

15. Zehnder, A.T. and Viz, M.J., "Fracture Mechanics of Thin Plates and Shells Under Combined Membrane, Bending, and Twisting Loads," *Applied Mechanics Reviews*, Vol. 58, 2005, pp. 37–48.

16. Wu, B.H. and Erdogan, F., "The Surface and Through Crack Problems in Orthotropic Plates," *International Journal of Solids and Structures*, Vol. 25, 1989, pp. 167–188.

17. Simmonds, J. and Duva, J., "Thickness Effects are Minor in the Energy Release Rate Integral for Bent Plates Containing Elliptic Holes or Cracks," *Journal of Applied Mechanics*, Vol. 48, 1981, pp. 320–326.

18. Awerbuch, J. and Madhukar, M.S., "Notched Strength of Composite Laminates: Predictions and Experiments—A Review," *Journal of Reinforced Plastics and Composites*, Vol. 4, 1985, pp 1–149.

19. Whitney, J.M. and Nuismer, R.J., "Stress Fracture Criteria for Laminated Composites Containing Stress Concentrations," *Journal of Composite Materials*, Vol. 8, 1974, pp. 253–265.

20. Nuismer, R.J. and Whitney, J.M., "Uniaxial Failure of Composite Laminates Containing Stress Concentrations," *ASTM STP 593*, 1975, pp. 117–142.

21. Poe, C.C. and Sova, J.A., "Fracture Toughness of Boron/Aluminum Laminates With Various Proportions of 0° and ±45° Plies," NASA Technical Paper 1707, 1980.

22. Poe, C.C., "A Unifying Strain Criterion for Fracture of Fibrous Composite Laminates," *Engineering Fracture Mechanics*, Vol. 17, 1983, pp. 153–171.

23. Mar, J.W. and Lin, K.Y., "Fracture Mechanics Correlation for Tensile Failure of Filamentary Composites With Holes," *Journal of Aircraft*, Vol. 14, 1977, pp. 703–704.

24. Lin, K.Y. and Mar, J.W., "Finite Element Analysis of Stress Intensity Factors for Cracks at a Biomaterial Interface," *International Journal of Fracture*, Vol. 12, 1987, pp. 521–531.

25. Costa, M.L., de Almeida, S.F.M., and Rezende, M.C., "The Influence of Porosity on the Interlaminar Shear Strength of Carbon/Epoxy and Carbon/Bismaleimide Fabric Laminates," *Composites Science and Technology*, Vol. 61, No. 14, November 2001, pp. 2101–2108.

26. Ashwell, A.G., "The Anticlastic Curvature of Rectangular Beams and Plates," *Journal of the Royal Aeronautical Society*, Vol. 54, 1950, pp. 708–715.

27. Kaldor, S.K. and Noyan, I.C., "Flexural Loading of Rectangular Si Beams and Plates," *Materials Science and Engineering A*, Vol. 399, 2005, pp. 64–71.

28. Chattopadhyay, L., "Analytical Solution for an Orthotropic Plate Containing Cracks," *International Journal of Fracture*, Vol. 134, 2005, pp. 305–317.

29. Walker, T.H., Avery, W.B., Ilcewicz, L.B., and Poe, C.C., "Tension Fracture of Laminates for Transport Fuselage – Part 1: Material Screening," *Second NASA Advanced Technology Conference*, NASA CP3154, 1991, pp. 197–238.

30. Walker, T.H., Ilcewicz, L.B., Polland, D.R., and Poe, C.C., "Tension Fracture of Laminates for Transport Fuselage – Part 2: Large Notches," *Third NASA Advanced Technology Conference*, NASA CP 3178, 1992, pp. 727–758.

31. Ilcewicz, L.B., Walker, T.H., Murphy, D.P., Dopker, B., and Scholz, D.B., "Tension Fracture of Laminates for Transport Fuselage – Part 4: Damage Tolerance Analysis," *Fourth NASA Advanced Technology Conference*, NASA CP 3229, 1993, pp. 264–298.

32. Backlund, J. and Aronsson C.G., "Tensile Fracture of Laminates With Holes," *Journal of Composite Materials*, Vol. 20, 1986, pp. 259–286.

33. Aronsson, C.G. and Backlund, J., "Tensile Fracture of Laminates With Cracks," *Journal of Composite Materials*, Vol. 20, 1986, pp. 287–307.

34. Dopker, B., Murphy, D.P., Ilcewicz, L.B., and Walker, T.H., "Damage Tolerance Analysis of Composite Transport Fuselage Structure," *35th AIAA/ASME/ASCE/AHS/ASC Structures, Structural Dynamics, and Materials Conference*, Hilton Head, South Carolina, 1994, pp. 58A-1–58A-8.

35. Kennedy, T.C. and Nahan, M.F., "A Simple Nonlocal Damage Model for Predicting Failure of Notched Laminates," *Composite Structures*, Vol. 35, 1996, pp. 229–236.

36. Kennedy, T.C. and Nahan, M.F., "A Simple Nonlocal Damage Model for Predicting Failure in a Composite Shell Containing a Crack," *Composite Structures*, Vol. 39, 1997, pp. 85–91.

37. *ABAQUS Analysis User's Manual*, Version 6.7, Simulia, Providence, Rhode Island, 2007.

38. Matzenmiller, A., Lubliner, J., and Taylor, R.L., “A Constitutive Model for Anisotropic Damage in Fiber-Composites,” *Mechanics of Materials*, Vol. 20, 1995, pp. 125–152.

39. Hashin, Z. and Rotem, A., “A Fatigue Criterion for Fiber-Reinforced Materials,” *Journal of Composite Materials*, Vol. 7, 1973, pp. 448–464.

40. Hashin, Z., “Failure Criteria for Unidirectional Fiber Composites,” *Journal of Applied Mechanics*, Vol. 47, 1980, pp. 329–334.

41. Camanho, P.P. and Davila, C.G., “Mixed-Mode Decohesion Finite Elements for the Simulation of Delamination in Composite Materials,” NASA/TM-2002-211737, 2002, pp. 1–37.

42. Hillerborg, A., Modeer, M., and Petersson, P.E., “Analysis of Crack Formation and Crack Growth in Concrete by Means of Fracture Mechanics and Finite Elements,” *Cement Concrete Research*, Vol. 6, 1976, pp. 773–782.

43. Krueger, R., “Virtual Crack Closure Technique: History, Approach, and Applications,” *Applied Mechanics Reviews*, Vol. 57, 2004, pp. 109–143.

44. Maimi, P., Camanho, P.P., Mayugo, J.A., and Davila, C.G., “A Thermodynamically Consistent Damage Model for Advanced Composites, NASA/TM-2006-214282, 2006.

45. Montgomery, D.C., *Design and Analysis of Experiments*, John Wiley & Sons, New York, 1997, pp. 693.

46. Mason, R.L., Gunst, R.F., and Hess, J.L., *Statistical Design and Analysis of Experiments*, John Wiley & Sons, New York, 1989, pp. 132–133.